SPECIAL ISSUE ARTICLE

The Anatomical Record WILEY

Evolutionary treasures hidden in the West Indies: Comparative osteology and visceral morphology reveals intricate miniaturization in the insular genera *Mitophis* Hedges, Adalsteinsson, & Branch, 2009 and *Tetracheilostoma* Jan, 1861 (Leptotyphlopidae: Epictinae: Tetracheilostomina)

Angele Martins[1,2] | Claudia Koch[3] | Mitali Joshi[3] | Roberta Pinto[4] | Alessandra Machado[5] | Ricardo Lopes[5] | Paulo Passos[2]

[1]Departamento de Ciências Fisiológicas, Universidade de Brasília, Brasília, Brazil

[2]Departamento de Vertebrados, Museu Nacional, Universidade Federal do Rio de Janeiro, Rio de Janeiro, Brazil

[3]Zoologisches Forschungsmuseum Alexander Koenig, Bonn, Germany

[4]Laboratório de Diversidade de Anfíbios e Répteis, Museu de Arqueologia da Universidade Católica de Pernambuco, Universidade Católica de Pernambuco, Recife, Brazil

[5]Instituto Alberto Luiz Coimbra de Pós-Graduação e Pesquisa em Engenharia, Laboratório de Instrumentação Nuclear, Universidade Federal do Rio de Janeiro, Rio de Janeiro, Brazil

Correspondence

Angele Martins, Laboratório de Anatomia Comparada de Vertebrados, Departamento de Ciências Fisiológicas, Instituto de Ciências Biológicas, Campus Darcy Ribeiro, Universidade de Brasília, Asa Norte, Brasília 70910-900, Distrito Federal, Brazil.
Email: amartins@unb.br

Abstract

The genera *Mitophis* and *Tetracheilostoma* comprise two extant lineages of small-sized threadsnakes that exclusively inhabit several islands of the West Indies. Even though leptotyphlopids are known for their extremely reduced size, miniaturization has only been hypothesized to reflect insular dwarfism for the genus *Tetracheilostoma*. Herein, we aim to describe the comparative osteology and visceral morphology of both genera, investigating and discussing their several internal morphological simplifications and novelties. Our results indicate that these taxa exhibit several autapomorphies mostly concentrated in the dorsoposterior skull elements and maxillae, as well as in their axial skeleton and viscera. These novelties and simplifications are most likely a result of extreme miniaturization driven by the evolutionary constraints or ecological opportunities possibly imposed by the "island rule." Both *Mitophis* and *Tetracheilostoma* distinguish from all other Epictinae in lacking a dentigerous process in the maxillae, by having the prootic fused to the otooccipital, and by the lack (except in comparison to a few *Epictia*) of a cervical vertebrae intercentrum I. Additionally, *Mitophis* can be distinguished from other Epictinae by the participation of the unpaired supraoccipital in the dorsal border of the foramen magnum, by the absence of the pleurapophyses in the caudal vertebrae, by a higher number of liver segments, and by the extreme degeneration of the pelvic rudiments. *Tetracheilostoma* differs from other Epictinae by lacking a distinct supraoccipital, which is fused to the parietal. Thus, our results reinforce that morphological

characters are extremely valuable for leptotyphlopid systematics given their extremely conserved external morphology.

1 | INTRODUCTION

Robert L. Stevenson published his famous novel "*Treasure Island*" in 1883 (formerly "*The Sea Cook: A Story for Boys*"), narrating the first modern buccaneer's tale. Its influence on popular perceptions of pirates was tremendous, including key narrative elements thereafter, such as maps tracking for destination of buried treasures. Islands are known to encompass many of the emerging topics on evolution, from both microevolutionary and macroevolutionary perspectives (Gould, 2002), representing true evolutionary laboratories for issues that can be difficult to investigate in more complex ecosystems (Grant, 1998; Losos, 2011; MacArthur & Wilson, 2001; Schluter, 1988). Among the best-documented insular patterns is the "island rule" (Van Valen, 1973), which describes the different tendencies among taxonomic groups toward dwarfism or gigantism in comparison with their mainland relatives (Foster, 1964; Lomolino, 1985; Van Valen, 1973). Lomolino (2005) reinforced that the "island rule" appears to be a general widespread phenomenon affecting lineages of nonvolant mammals, bats, passerine birds, snakes and turtles, where usually large species (e.g., elephants) are smaller on islands and small species (e.g., rodents) are larger. Even though there seems to be a debate on whether the island rule is valid for all vertebrate taxa (see Benton et al., 2010), one of the main conclusions is that the body-size of numerous vertebrate species varies significantly with island isolation and island area.

Snakes are very successful island inhabitants and there is extensive scientific literature on their island-based natural history (reviewed in Lillywhite & Martins, 2019). For instance, studies on island snakes add important discoveries to the knowledge of various evolutionary processes, such as: gigantism, the evolution of convergent phenotypes and new ecological opportunities (e.g., Card et al., 2016; Esquerré et al., 2020; Keogh, Scott, & Hayes, 2005). Martins and Lillywhite (2019) emphasize that there are numerous reasons why snakes are important elements in island biotas, playing critical roles on numerous islands (continental or oceanic), therefore offering more information for understanding the ecology of islands and the evolution of nsular taxa in general. Some of the most important attributes of snakes related to success in island occupation and permanence are: ectothermy and comparatively lower energy demands compared to other groups of vertebrates; unique morphofunctional and ecophysiological features that favor the ability to disperse over water (e.g., locomotion pattern with low energy); different life-styles (e.g., fossorial, arboreal, semi-aquatic) and occupation of different ecological niches, minimizing interspecific competition; life history characteristics that favor comparatively rapid population growth (e.g., viviparity, development of multiple litters); variety in body sizes and shapes favorable to the occupation even of very small islands; breadth and plasticity of the diet, including elimination; effective means of acquiring prey (e.g., envenomation, constriction); consumption of relatively large prey and slow digestive physiology; disruptive behaviors and cryptic morphologies, avoiding visually oriented predators; scansorially specialized phenotypic traits in many species (e.g., prehensile tail, posteriorly curved teeth); thermal plasticity and complex thermoregulatory behavior; and a wide repertoire of antipredator defensive tactics associated with distinct activity patterns (Martins & Lillywhite, 2019, and references therein).

The subtribe Tetracheilostomina comprises two extant leptotyphlopid genera: *Mitophis* Hedges, Adalsteinsson & Branch, 2009, containing four species distributed on the Greater Antillean islands of Hispaniola, including the countries of the Dominican Republic and Haiti; and *Tetracheilostoma* Jan, 1861 with three species distributed on the Lesser Antillean islands of Martinique, Saint Lucia and Barbados (Adalsteinsson, Branch, Trape, Vitt, & Hedges, 2009; Uetz, Freed, & Hosek, 2020). Similar to other leptotyphlopid lineages, members of the subtribe Tetracheilostomina exhibit a generally conserved external morphology, leading to taxonomic uncertainty for inferring species boundaries (Boulenger, 1893; Thomas, 1965; Thomas, McDiarmid, & Thompson, 1985; Underwood, 1963). On the other hand, differing from other Caribbean scolecophidians, Hedges (2008) found that in the case of members of the genus *Tetracheilostoma*, species reach the low extreme limits of snake body length (maximum snout-vent length of 105 mm). Members of *Mitophis*, at the same time, reach the lower limit of maximum body width among known leptotyphlopids, with very thin bodies (2.5 mm; Adalsteinsson et al., 2009; Thomas et al., 1985). This pattern contrasts with the general widespread tendency according to the island rule for small-sized lineages of terrestrial

vertebrates to become larger (Lomolino, 2005), and perhaps may be related to new ecological opportunities and open niches normally occupied by small-sized invertebrates on the mainland (Hedges, 2008; Millien, 2006).

Taking advantage of external morphology and molecular evidence provided by Hedges (2008), Adalsteinsson et al. (2009), and Martins, Koch, et al. (2019), we aim to investigate if there are further phenotypic changes involving the baupläne of members of the subtribe Tetracheilostomina. In this sense, we aim to provide detailed comparisons of the osteology for the species of the insular endemic genera, *Mitophis* and *Tetracheilostoma*, which represent true underground evolutionary treasures hidden on the Caribbean islands. We also describe intraspecific variation in the osteology and visceral data for *Mitophis leptepileptus* and *Tetracheilostoma bilineata*.

2 | MATERIALS AND METHODS

We examined a sample of 31 specimens covering all seven species of Tetracheilostomina (i.e., *Mitophis* and *Tetracheilostoma*) housed in the following collections: United States National Museum, Smithsonian Institution, Washington, DC (USNM); Kansas University, Lawrence, USA (KU); Museum of Comparative Zoology, Cambridge, USA (MCZ); Natural History Museum, London, UK (NHMUK); Muséum National d'Histoire Naturelle, Paris, France (MNHN); and Zoological Collection of the Museum für Naturkunde, Berlin, Germany (ZMB). We provide information on the specimens and localities in the Material Examined section. We were able to assess data on the skull, lower jaw, and cervical morphology of one species (*M. leptepileptus*) of the four currently recognized *Mitophis* spp.; and from two *Tetracheilostoma* (*T. bilineata* and *T. carlae*) of the three currently recognized species in the genus (see Uetz et al., 2020). Osteological data were obtained through images of the skull, lower jaw, and postcranial skeleton of six specimens (corresponding to three species) with the aid of high-resolution micro-computed tomography (μCT) scanning procedures using a Bruker SkyScan 1176 High Resolution in vivo μCT available at Universidade de São Paulo, São Paulo, a Bruker SkyScan 1173 or SkyScan 1272, available at the Zoological Research Museum Alexander Koenig (ZFMK), Bonn (for the specimens of *Tetracheilostoma*) and a Bruker Skyscan 1273 at Instituto Alberto Luiz Coimbra de Pós-graduação e Pesquisa de Engenharia (COPPE), Laboratório de Instrumentação Nuclear, Universidade Federal do Rio de Janeir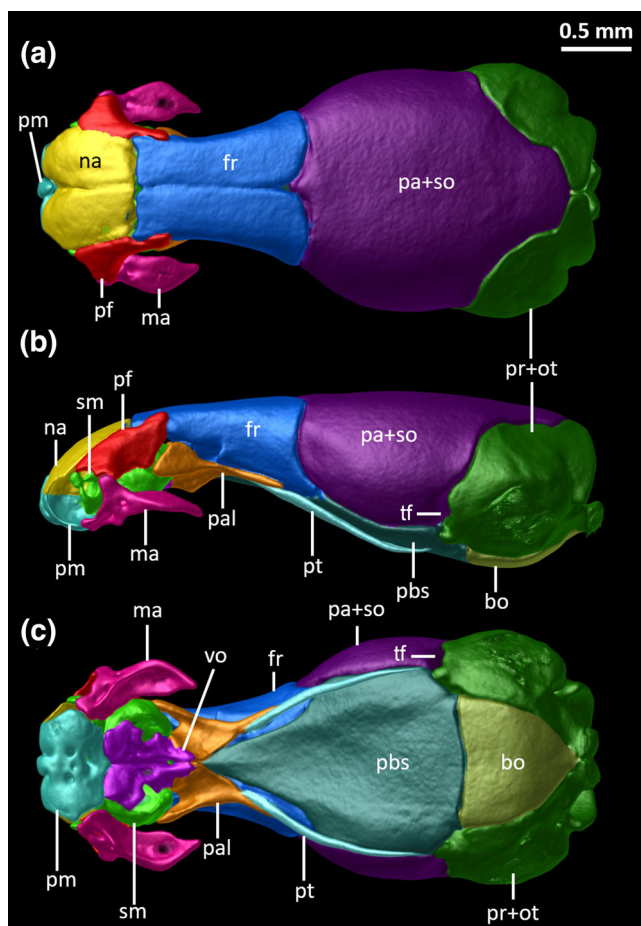o, Rio de Janeiro. The scans were conducted using an X-ray beam with 30–45 kV source voltage and 114–200 μA current without the use of a filter. Rotation steps of 0.25–0.4° were used with a frame averaging of 4–6, recorded over a 180° rotation, resulting in 482–960 projections of 280–904 ms exposure time each and a total scan duration of 0 hr:25 m:39 s–1 hr:11 m:42 s. The magnification setup generated data with an isotropic voxel size of 6.0–21.3 μm. We used Amira visualization software (ThermoFisher Scientific) for segmentation and to generate colored images of one specimen of *T. bilineata* and of *M. lepitepileptus*. Additional images were visualized in CTVox for Windows 64bit version 2.6 (Bruker, μCT), and plates were made using Inkscape 1.0. Additionally, one specimen of *M. leptepileptus* was cleared and stained for both osteological and cartilaginous data based on the protocols of Taylor and Van Dyke (1985) and Song and Parenti (1995). We were able to assess general morphological data (mostly quantitative) for all currently recognized species of *Mitophis* and *Tetracheilostoma* based on radiographic images through a Kevex PXS10-16W 130 kVp 6 *Micron Spot MicroFocus X-Ray Source* at the USNM. Images were generated through the software KEVEX X-RAY *Source Control Interface* version 5.5.9 (see Material Examined). When possible, type specimens (mainly holotypes and paratypes) from each species were considered for descriptions and are indicated in the Material Examined. The raw data are available from the authors upon request. Finally, we also gathered morphological and topographical data of viscera by the dissection of one male specimen of *M. leptepileptus*, and three female specimens of *T. bilineata*.

Anatomical terminology follows Rieppel, Kley, and Maisano (2009) for skull; Kley (2006) for lower jaw; and Holman (2000) for vertebrae. We follow Wallach (1998a, 1998b) for visceral terminology, and visceral data (e.g., length, gap, and interval) are provided as % of the snout-vent length. We identified the specimens based on the original descriptions and taxonomic studies addressing tetracheilostomine taxonomy, such as: Thomas (1965), Thomas et al. (1985), Hedges (2008), and Adalsteinsson et al. (2009). The supraspecific taxonomy adopted herein follows Wallach, Williams, and Boundy (2014) and Uetz et al. (2020). Intra- and inter-specific variation is indicated within their respective descriptive sections, always accompanied by the percentage of specimens exhibiting such condition. As not all characters were distinguishable or observable in all examined specimens, the "*n*" and/or the percentage relates to the number of specimens of which the related character was analyzed, and thus will not always represent the total sample examined.
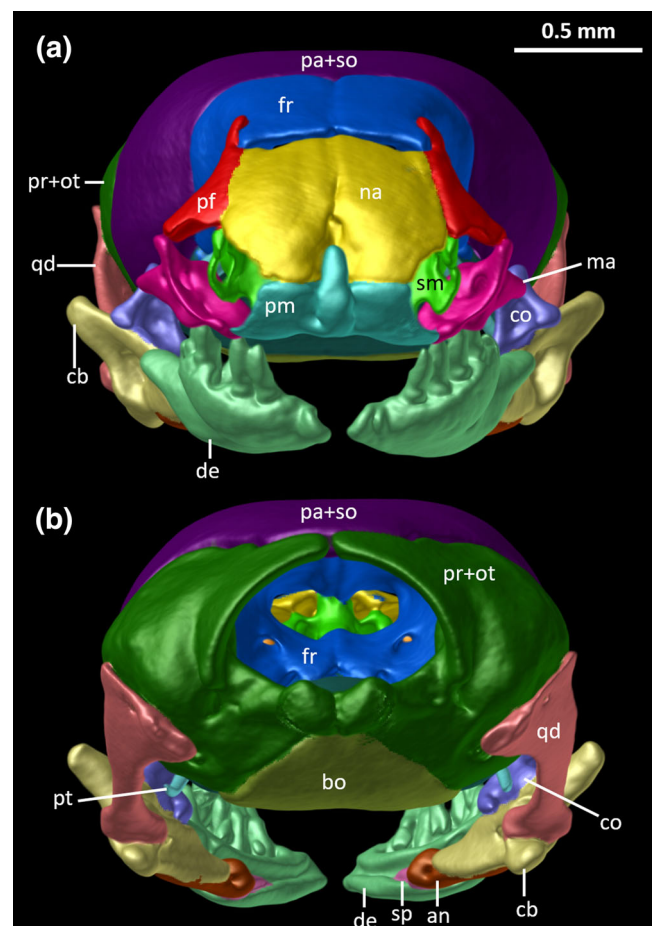
3 | RESULTS

3.1 | Skull morphology of *Mitophis* and *Tetracheilostoma*

The skulls of members of the genera *Mitophis* and *Tetracheilostoma* are deeply ossified, longer than wide, and dorsoventrally flattened, with elements organized in the following regions: (a) snout complex, (b) palatomaxillary apparatus (= upper jaw), (c) braincase and orbital complex, and (d) otic capsule (Figures 1–11). The skull of *Mitophis* is more dorsoventrally flattened both anteriorly and posteriorly in comparison with *Tetracheilostoma* (Figures 1 and 9).

The snout complex is composed of the premaxilla, nasals, prefrontals, septomaxillae, and vomers. In *Tetracheilostoma*, this complex is slightly thinner than the widest region of the braincase (parietal). All elements are partially overlapped (i.e., telescoped; Figures 1–3, 9–11) at some level, resulting in a robust and akinetic snout complex. The nares are anterolaterally oriented (Figures 1b, 2a, 8, 9b, and 10a) and limited by the premaxilla anteriorly and ventrally, the septomaxilla posteriorly, and the nasal dorsally (Figures 1–2, 8–10). In *T. bilineata*, the maxillae participate in a short portion of the lateroventral margin of the nares (Figures 1 and 8e–p), but in *T. carlae* (Figure 8a–d) and *M. leptepileptus*
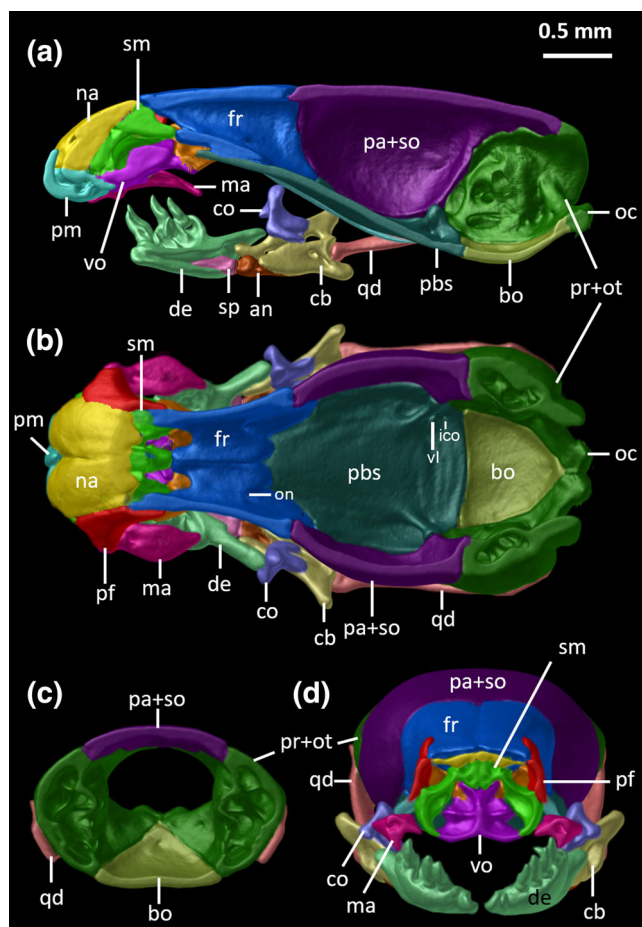

FIGURE 1 Dorsal (a), lateral (b), and ventral (c) views of the three-dimensional reconstruction of the skull of *Tetracheilostoma bilineata* (BMNH 1853.2.4.36) based on μCT data. Different skull elements are digitally colored to improve visualization of elements, and the mandibles and quadrates were digitally removed for better visualization. Abbreviations are as follows: bo, basioccipital; fr, frontal; ma, maxilla; na, nasal; pa + so, fused parietal and supraoccipitals; pal, palatine; pbs, parabasisphenoid; pf, prefrontal; pm, premaxilla; pr + ot, fused prootic+otooccipital; pt, pterygoid; sm, septomaxilla; tf, trigeminal nerve foramen; vo, vomer

FIGURE 2 Anterior (a) and posterior (b) views of the three-dimensional reconstruction of the skull and lower jaw (suspensorium + mandible) of *Tetracheilostoma bilineata* (BMNH 1853.2.4.36) based on μCT data. Different skull elements are digitally colored to improve visualization of elements. Abbreviations are as follows: an, angular; bo, basioccipital; cb, compound bone; co, coronoid; de, dentary; fr, frontal; ma, maxilla; na, nasal; pa + so, fused parietal and supraoccipitals; pf, prefrontal; pm, premaxilla; pr + ot, fused prootic+otooccipital; pt, pterygoid; qd, quadrate; sp, splenial

FIGURE 3 Three-dimensional cutaway views along the sagittal (a), vertical (b), and transverse (c,d) axes of the skull of *Tetracheilostoma bilineata* (BMNH 1853.2.4.36) based on μCT data. Different skull elements are digitally colored to improve visualization of elements. Abbreviations are as follows: an, angular; bo, basioccipital; cb, compound bone; co, coronoid; de, dentary; fr, frontal; ico, internal carotid opening; ma, maxilla; na, nasal; oc, occipital condyle; on, optic nerve foramen; pa + so, fused parietal and supraoccipitals; pbs, parabasisphenoid; pf, prefrontal; pm, premaxilla; pr + ot, fused prootic+otooccipital; qd, quadrate; sm, septomaxilla; sp, splenial; vo, vomer

(Figure 9b) the maxillae are excluded from the formation of the nares by the dorsal expansion of the septomaxillae.

The palatomaxillary apparatus is composed of the paired maxillae, palatines, and pterygoids. An ectopterygoid is absent or indistinct.

The orbital complex is limited anteriorly by the prefrontals, medially by the frontals, and ventrally by the maxillae, with the frontals totally enclosing the optic nerve foramen. In *Tetracheilostoma*, the palatines seem to participate in the anteromedial wall of the orbital complex (Figure 1b). A posterior orbital element is absent.

The braincase is composed of the fused parietal, supraoccipitals (fused to parietal in *Tetracheilostoma* and

fused to each other in *Mitophis*), prootic fused to otooccipital (herein called fused prootic + otooccipital), parabasisphenoid complex, and basioccipital (Figures 1–3, 6–11). The otic capsule is completely delimited by the prootic + otooccipital in both *Mitophis* and *Tetracheilostoma* (Figures 3,11).

3.1.1 | Snout complex

The *premaxilla* (Figures 1–4, 9–11) is edentulous and forms the anteroventral portion of the snout complex. It contacts the nasals dorsally, the vomers ventroposteriorly, and the septomaxillae ventrolaterally. In *T. bilineata*, three ($n = 1$), four ($n = 1$), or five foramina ($n = 2$; Figure 4) pierce the anterior and/or ventral lamina of the premaxilla and give path to the rami of the *ophthalmicus profundus* nerve (V1; Haas, 1964; Rieppel et al., 2009); while in *T. carlae* it is perforated by a total of four foramina (Figure 8a,d). A total of five foramina pierce the ventral and anterior surfaces of the premaxilla of *M. leptepileptus* (Figure 9c). The anterior lamina of the premaxilla of both genera is approximately rectangular with concave lateral limits and a straight dorsal limit that contacts the nasals and is hardly visible in dorsal view (Figures 2, 4, and 5). A finger-like conspicuous medial process (possibly an internasal process) projects dorsally in all *Tetracheilostoma* and *Mitophis*, but this structure does not contact the nasals dorsally (Figures 2a, 8a,e,i,m, and 10a). In *Mitophis* the ventral lamina of the premaxilla is approximately trapezoidal (Figure 9), while in *Tetracheilostoma* it is approximately heptagonal (Figures 1 and 8). In *Tetracheilostoma*, the ventral lamina expands posteriorly into a small and inconspicuous tapered vomerine process (Figures 1c, 4b,e, and 8d,h,l,p) while such a process is absent in *Mitophis*, with the posterior limit being concave and covering the anterior portion of the vomers (Figure 9c).

The paired *nasals* (Figures 1–4, 8–11) are approximately rectangular, being slightly less than twice ($n = 1$; *T. carlae*), twice ($n = 2$; *T. bilineata*) or more than twice ($n = 2$; *T. bilineata*; *M. leptepileptus*) longer than wide in dorsal view. The nasals contact the premaxilla anteriorly and ventrally, the frontal posteriorly, the prefrontal lateroposteriorly, and the septomaxillae ventromedially (Figures 1–3, 8–11). The nasal-frontal suture is undulated ($n = 1$, *T. bilineata*, Figure 8n; $n = 1$, *T. carlae*, Figure 8B; *M. leptepileptus*, Figure 9a) or approximately straight ($n = 2$, *T. bilineata*, Figure 8f,j). The dorsal surface of the nasals is essentially convex, with each element projecting midventrally to form the paired nasal septum that is ventrally supported by the short medial (internal) lamina of the premaxilla (Figures 3a,d, 4g–i, and 11a,d).
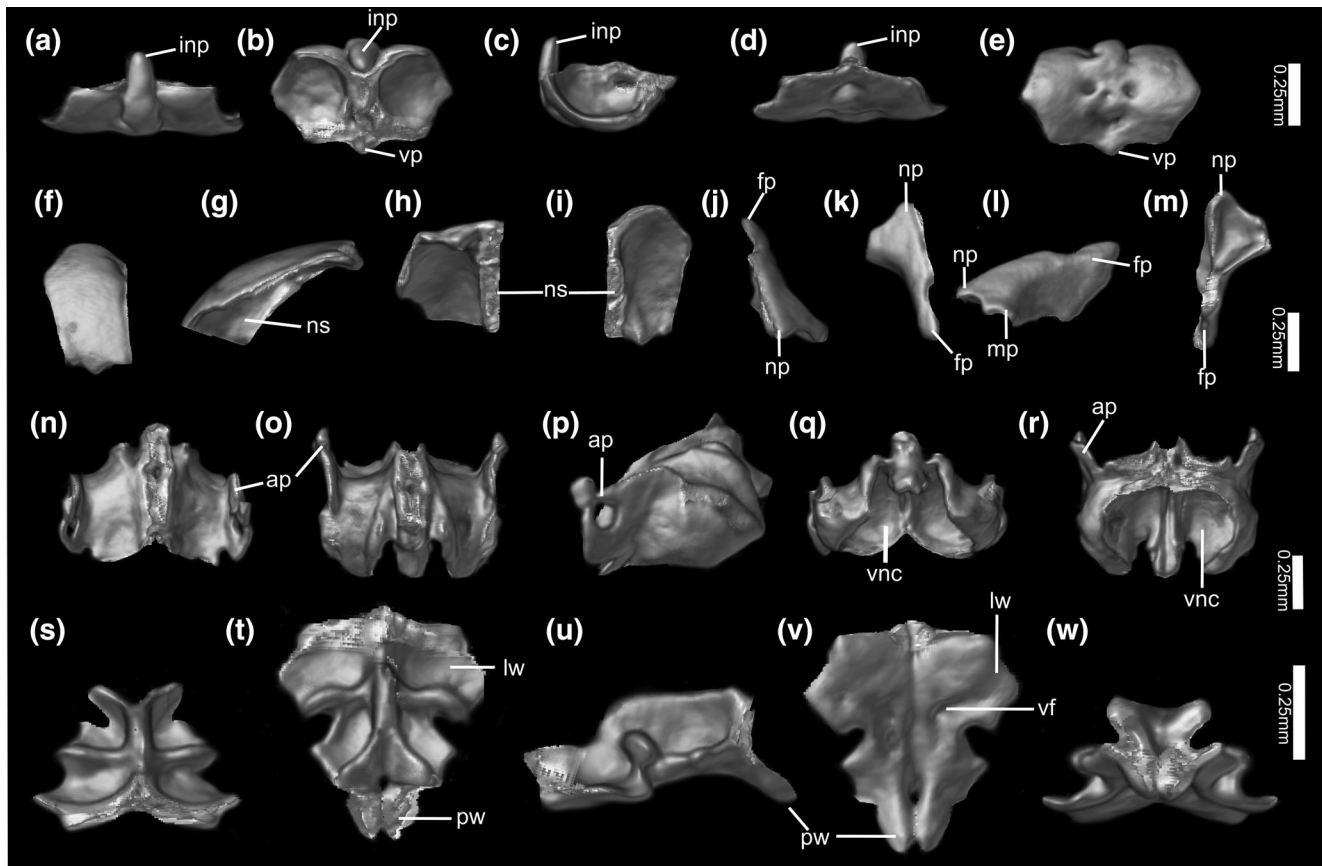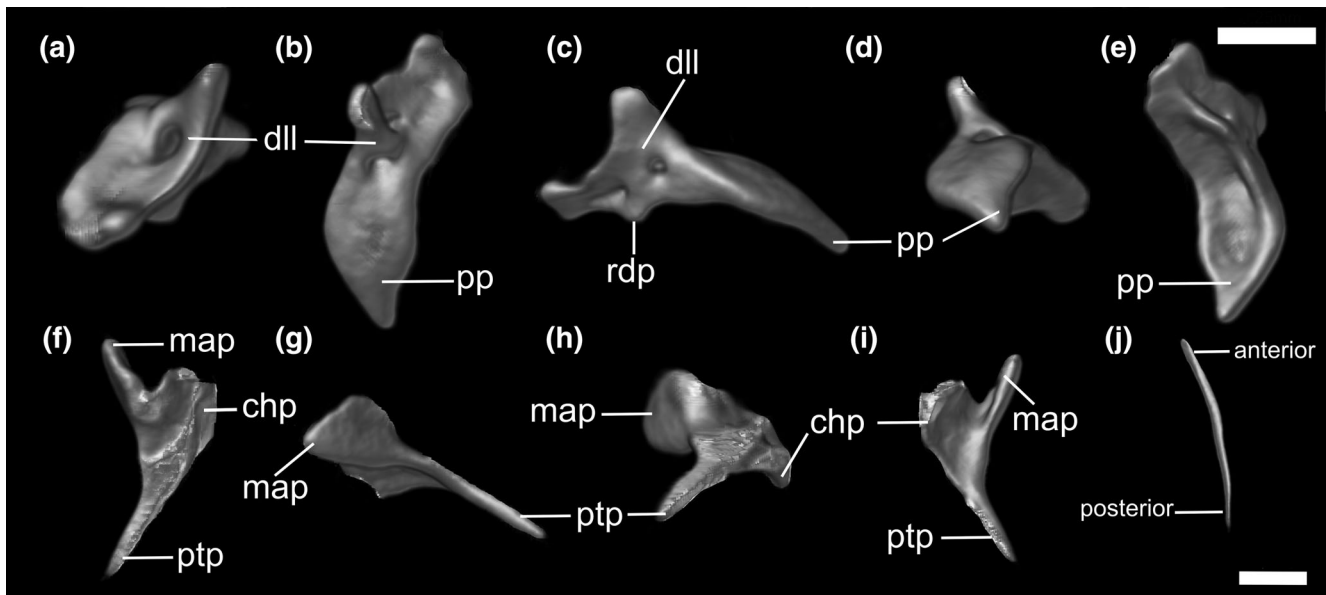
FIGURE 4 Three-dimensional reconstruction of digitally isolated bones of the snout complex of *Tetracheilostoma bilineata* (BMNH 1853.2.4.36) based on μCT data. Premaxilla in anterior (a), dorsal (b), lateral (c), posterior (d), and ventral (e) views. Nasal in dorsal (f), lateral (g), posterior (h), and ventral (i) views. Prefrontal in anterior (j), dorsal (k), lateral (l), and ventral (m) views. Septomaxillae in anterior (n), dorsal (o), lateral (p), posterior (q), and ventral (r) views. Vomers in anterior (s), dorsal (t), lateral (u), ventral (v), and posterior (w) views. Abbreviations are as follows: ap, ascending process; fp, frontal process; inp, internasal process; lw, lateral wing; mp, maxillary process; np, nasal process; ns, nasal septum; pw, posterior wing; vf, vomerine foramen; vnc, vomeronasal cupola; vp, vomerine process

In both *Tetracheilostoma* and *Mitophis*, each nasal, together with the frontals and a short inconspicuous lateral portion of the prefrontal, form the foramen for the *apicalis nasi* nerve (Figures 1a, 8b,f,j,n, and 9a).

The *prefrontals* (Figures 1–4, 8–11) are expanded laterally and concave medially, located at the lateral edge of the snout complex. Their dorsal lamina is approximately triangular (Figures 1a, 4k, 8b,f,j,n, 9a). Each element contacts the nasals, frontals and the ascending process of the septomaxilla medially, and in *Tetracheilostoma*, the maxilla ventrally (although in one specimen of *T. bilineata* the latter varies bilaterally; Figures 1–3, 8–11). Each prefrontal bears three processes (Figure 4j–m): (a) an anterior process (nasal process), (b) a posterior process (frontal process), and (c) a ventral process (maxillary process). Both nasal and frontal processes are respectively stout and elongate anterior and posterior projections, the former contacting the nasals and ascending process of the septomaxilla medially, and the latter contacting the frontals and septomaxillae ventrally (Figures 1–4, 8j–m,

9, and 10). In *Tetracheilostoma*, the maxillary process descends forming concave anteroventral and posteroventral surfaces together with the maxilla laterally and the ascending process of the septomaxilla anteroventrally (Figures 1b and 8c,g,k,o). In *Mitophis*, however, the maxillary process fails to contact the maxillae ventrally (Figure 9b). In *Tetracheilostoma*, the posterior lamina of the maxillary process is concave and delimits the optic capsule anteriorly (Figures 1,8).

The *septomaxillae* (Figures 1–4,8–11) are complex in shape, representing the main bony structure that encloses the vomeronasal organ. These elements are mostly visible in ventral view, and extend dorsolaterally toward the vomers, contacting all elements of the snout complex as well as the frontals. Each septomaxilla expands dorsolaterally to form an ascending process that slightly inflects medially toward the nasal septum (Figures 1–4, 9, and 11). This ascending process is perforated by a large anterior foramen that is ventral to a dorsal process that develops and fits ventrally into the nasal-prefrontal

FIGURE 5 Three-dimensional reconstruction of digitally isolated bones of the palatomaxillary apparatus of *Tetracheilostoma bilineata* (BMNH 1853.2.4.36) based on μCT data. Maxilla in anterior (a), dorsal (b), lateral (c), posterior (d), and ventral (e) views. Palatine in dorsal (f), lateral (g), posterior (h), and ventral (i) views. Pterygoid in ventral (j) view. Abbreviations are as follows: chp, choanal process; dll, dorsolateral lamina; map, maxillary process; pp, posterior process; ptp, pterygoid process; rdp, rudimentary dentigerous process. Scale on the top 0.25 mm and refers to maxilla; scale on the bottom is 0.25 mm to palatine and 0.5 mm for pterygoid

suture (Figure 4n–r). In one specimen of *T. bilineata*, this dorsal process is reduced and trapezoidal. Ventrally, the septomaxillae contact the vomers anteriorly (but not their posterior wings), surrounding the vomeronasal fenestra (Figures 1–4, 9, and 11). Medially (internally) each septomaxilla develops a wide lamina that forms the dorsal cover of the vomeronasal cupola (Figures 3, 4, and 11). In *Tetracheilostoma*, this lamina expands dorsoposteriorly and inflects medially (Figure 4n–r), forming the passage for the vomeronasal nerve together with the subolfactory process of the frontal (Figures 3b and 11b). The dorsal lamina of the septomaxilla contacts the premaxilla anteriorly and the nasal septum posteriorly (Figure 3d) in *Tetracheilostoma*. In *M. leptepileptus*, however, the septomaxilla also bears a dorsal flange that contacts the frontals ventrally (Figure 11d). In *T. bilineata*, the internal lamina is usually pierced by an anterior foramen that leads to the vomeronasal cupola ($n = 2$) or by two foramina that lead to the internal aspect of the premaxilla ($n = 1$). In *T. carlae*, no distinct foramina are found in the dorsal (internal) lamina of the septomaxilla. A sulcus for the medial *ophthalmicus profundus* (VI) is absent or indistinct in the dorsal surface (Figure 4n–o) of all *Tetracheilostoma* analyzed herein, but present and conspicuous in *M. leptepileptus*.

The *vomers* (Figures 1, 3, 4, 8, 9, and 11) are small elements located midventrally to the vomeronasal cupola, completing the medial margin of the ventral opening of the vomeronasal organ (*fenestra vomeronasalis*). Each vomer is pierced by a vomerine foramen (Figure 4v), and contacts the premaxilla anteriorly, the septomaxilla anterolaterally, and the palatine posteriorly (Figures 1, 3, 4, 8, 9, and 11). In *Tetracheilostoma*, the lateral wing (Figure 4t,v) of each vomer is wide and bends dorsally (internally) onto the vomeronasal cupola into an anteroposteriorly flattened and rectangular ($n = 3$) or subtriangular process ($n = 1$). A posterior process (= posterior wing; Figure 4t–v) is also present in each vomer, extending posteriorly to contact the palatines laterally (Figures 1c, 8d,h,l,p, and 9c). In *T. bilineata*, these wings are in medial contact with each other along their entire extension ($n = 2$) or only at their posterior half ($n = 2$; Figure 4v); while in *T. carlae* these wings are medially separated by a conspicuous gap (Figure 4d). In *M. leptepileptus* ($n = 1$), the posterior wings are medially separated by an inconspicuous gap (Figure 9c).

3.1.2 | Palatomaxillary apparatus

The *maxillae* (Figures 1–3, and 9) are irregular and edentulous bones that are longitudinally oriented to the skull. In *Tetracheilostoma*, each maxilla provides a small ventrolateral cover for the snout complex, being connected to both the premaxilla midventrally and the prefrontal dorsally (Figures 1–3). In *Mitophis*, the maxillae are
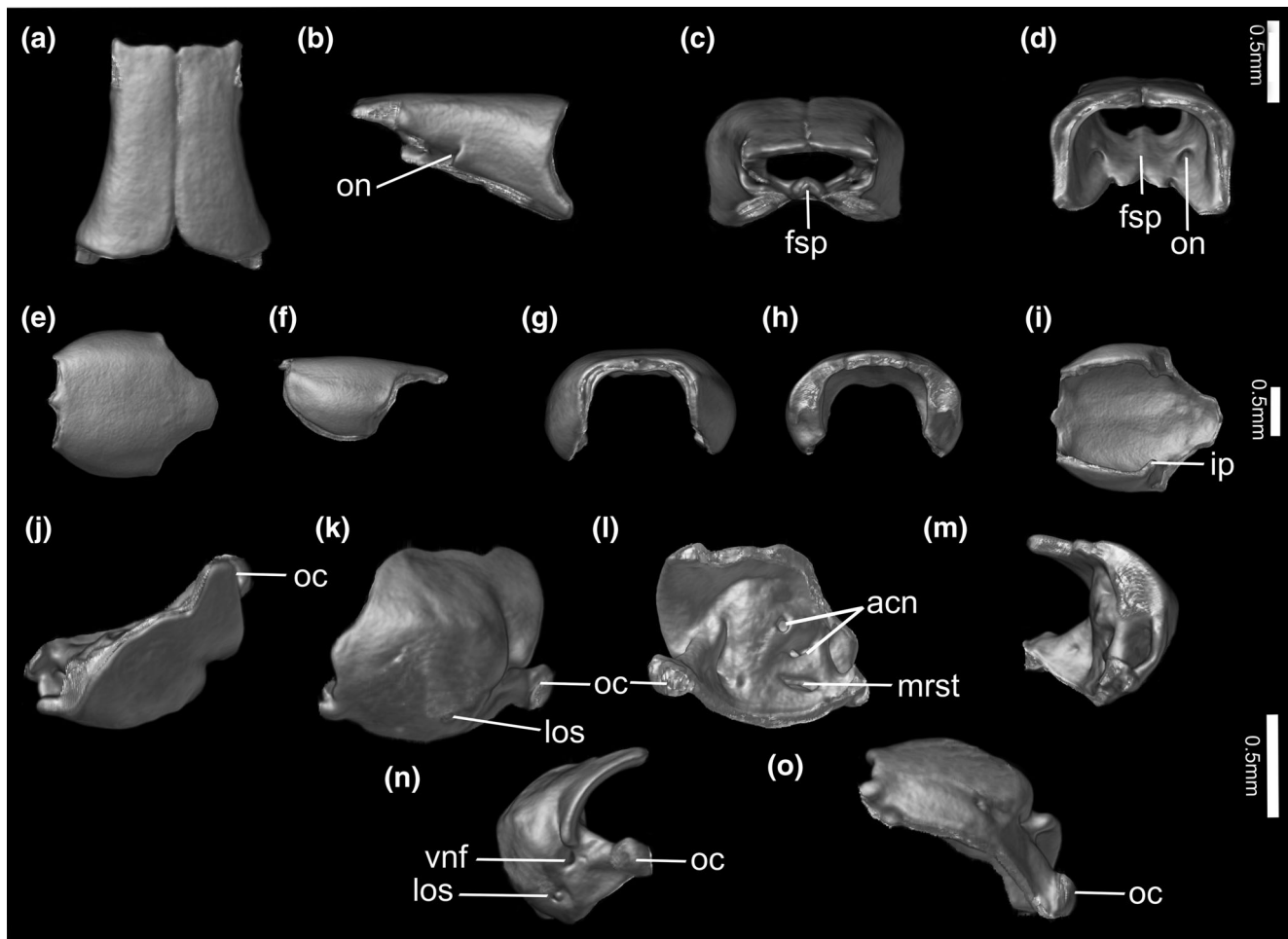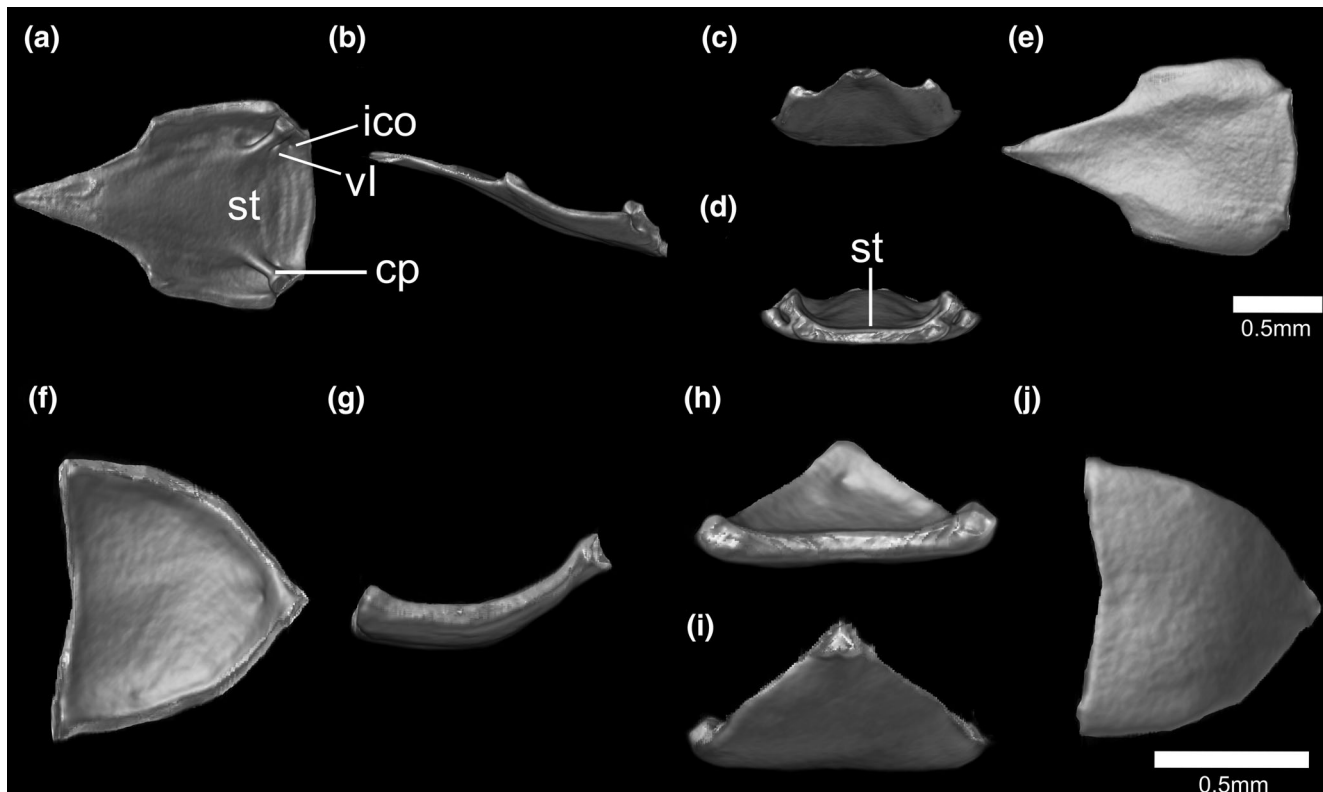
FIGURE 6 Three-dimensional reconstruction of digitally isolated bones of the orbital complex, braincase and otic capsule of *Tetracheilostoma bilineata* (BMNH 1853.2.4.36) based on μCT data. Frontals in dorsal (a), lateral (b), anterior (c), and posterior (d) views. Fused parietal and supraoccipital in dorsal (e), lateral (f), anterior (g), posterior (h), and ventral (i) views. Fused otooccipital and prootic in dorsal (j), lateral (k), medial (l), anterior (m), posterior (n), and ventral (o) views. Abbreviations are as follows: acn, acoustic nerve foramina; fsp, frontal subolfactory process; ip, internal pillar; los, lateral opening for the stapes; mrst, medial aperture for the recessus scalae tympani; oc, occipital condyle; on, optic nerve foramen; vnf, vagus nerve foramen

extremely reduced (Figure 9b), connected exclusively to the premaxilla (Figure 9c), and composed by: (a) a laminar element comprising a reduced, rectangular and laterally compressed anterior process, and (b) a rod-like and dorsoventrally flattened posterior process. In *Tetracheilostoma*, two distinct processes might be distinguishable in each maxilla (Figures 1–3, and 5a–e): (a) a dorsolateral lamina that abuts to the prefrontal through a dorsal subtriangular process and to the premaxilla by a reduced dorsoanterior process respectively, being perforated by a few foramina that may vary bilaterally from one ($n = 2$ sides), two ($n = 2$ sides), or three ($n = 1$ side); and (b) a posterior tapered process that is dorsoventrally compressed, extending posteriorly and medially reaching ($n = 2$; Figure 8c,g) or not ($n = 2$; Figure 8k,o) the level of the optic foramen in lateral view. A dentigerous

process is absent in *T. carlae* and one specimen of *T. bilineata* (Figure 8c,g), although two specimens of *T. bilineata* (Figure 8k,o) display an inconspicuous ventral expansion that might represent a rudimentary dentigerous process (Figure 5c). The dorsolateral lamina in *Tetracheilostoma* is undeveloped and concave anteriorly, exposing a wide portion of the ascending process of the septomaxilla in lateral view (Figures 1b and 8c,g,k,o). In *M. leptepileptus* this lamina is absent (Figure 9b).

The *palatines* (Figures 1,5,8–9) are triradiate, located lateroventrally to the anterior portion of the skull. In *Tetracheilostoma*, each element is composed of three processes (Figure 5f–i), described as follows. The maxillary process (a) is stout and abuts to the posterior wall of the septomaxilla anteriorly and the frontal dorsally (Figures 1b,c, 8, and 9b,c) in *Tetracheilostoma*, while in

FIGURE 7 Three-dimensional reconstruction of digitally isolated bones of the basicranium of *Tetracheilostoma bilineata* (BMNH 1853.2.4.36) based on μCT data. Parabasisphenoid in dorsal (a), lateral (b), anterior (c), posterior (d), and ventral (e) views. Basioccipital in dorsal (f), lateral (g), anterior (h), posterior (i), and ventral (j) views. Abbreviations are as follows: cp, clinoid process; ico, internal carotid opening foramen; st, sella turcica; vI, abducens nerve (VI) foramen

Mitophis it is quadrangular and does not contact any bone anteriorly. The choanal process (b) is a medial and dorsoventrally flattened projection that inflects ventrally to contact the posterior wing of the vomer (Figures 1c, 5f–i, and 8d,h,l,p). These processes are each perforated by a foramen and contact each other medially (Figures 1c, 8d,h,l,p, 9c). The pterygoid process of the palatine (c) is a rod-like posterior process that medially abuts to a short anterior region of the pterygoid (Figures 1c, 5f–i, 8d,h,l,p, and 9).

The *pterygoids* (Figures 1, 3, 5, and 9) are slender rod-like bones that extend throughout the ventral and lateral portion of the skull, from the level of the anterior portion of the parabasisphenoid, reaching posteriorly the level of the trigeminal nerve foramen (*T. bilineata*; Figures 1c and 8h,l,p) or ending anterior to it (*T. carlae*, Figure 8d; *M. leptepileptus*, Figure 9c). Each pterygoid slightly bends medially throughout its posterior extension (Figure 5j), being exclusively in contact with the pterygoid process of the palatine anteriorly (Figures 1a and 9a), and with its whole posterior extension being suspended from the skull by the *Musculus protractor pterygoidei* (Martins, Passos, & Pinto, 2019).

3.1.3 | Orbital complex, braincase, and otic capsule

The prefrontals, maxillae, palatines, and the frontals contribute to the orbital complex, but have been described above. A posterior orbital element is absent. The braincase is composed of the parietal, the fused supraoccipitals (distinct in *Mitophis* but fused to parietal in *Tetracheilostoma*), the prootic + otooccipital (fused), the parabasisphenoid complex, and the basioccipital.

The *frontals* (Figures 1–3, 6, and 8–11) are wide elements that form a conspicuous anterior area of the skull, being about three times (n = 3, *T. bilineata*, Figure 8f,j,n; n = 1, *M. leptepileptus*, Figure 9a) or four times (n = 1, *T. bilineata*, Figure 1a; n = 1, *T. carlae*, Figure 8b) longer than wide. Each frontal is nearly rectangular in dorsal view, with an inconspicuously undulated anterior limit and a convex posterior limit (Figures 1a, 6a, and 9a). These elements contact the posterior margin of the nasal anteriorly and the anterior margin of the parietal posteriorly, descending to contact the parabasisphenoid, septomaxilla and nasal septum ventrally (Figures 3, 6a–d, and 11). A reduced anterolateral projection that fits to
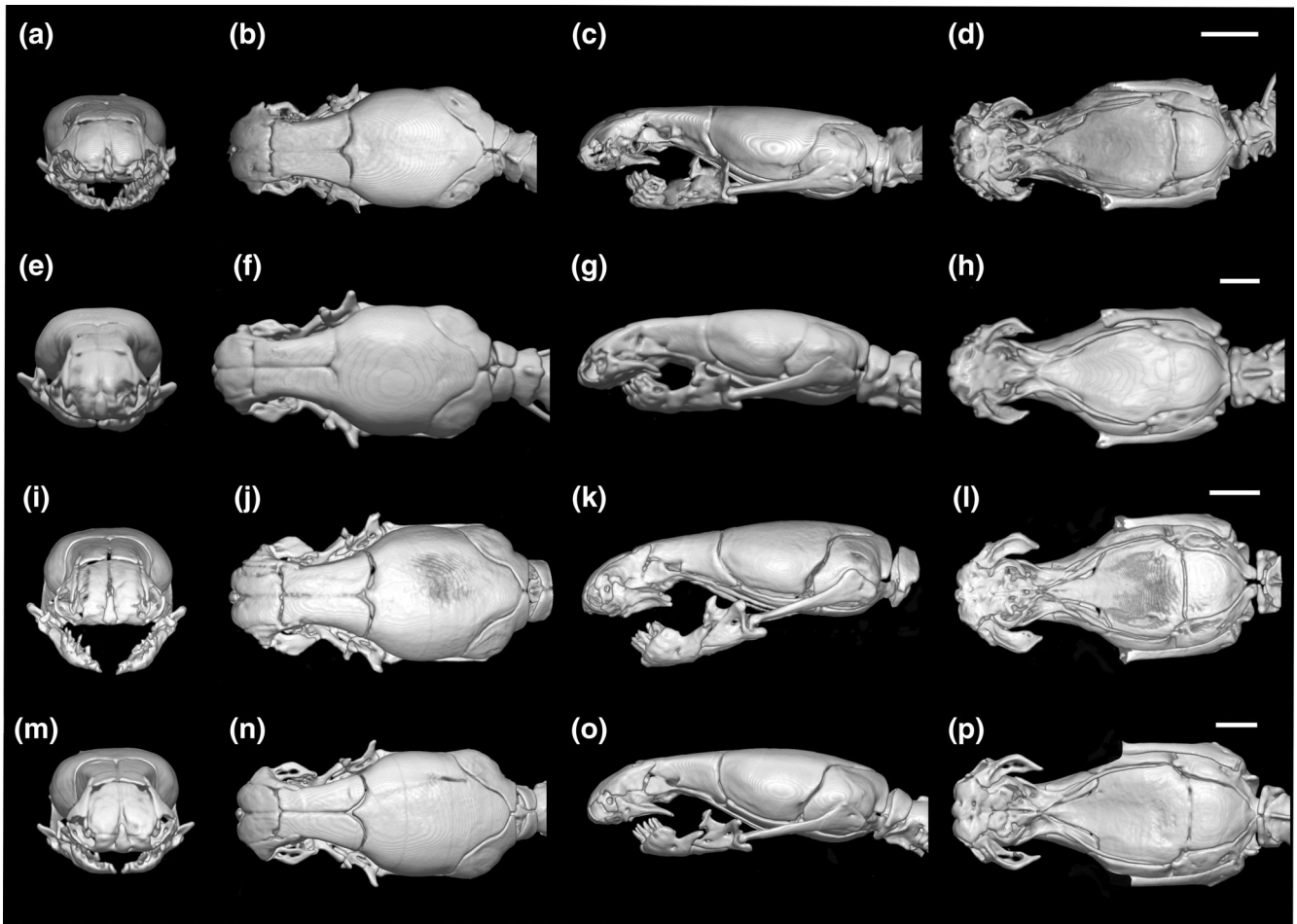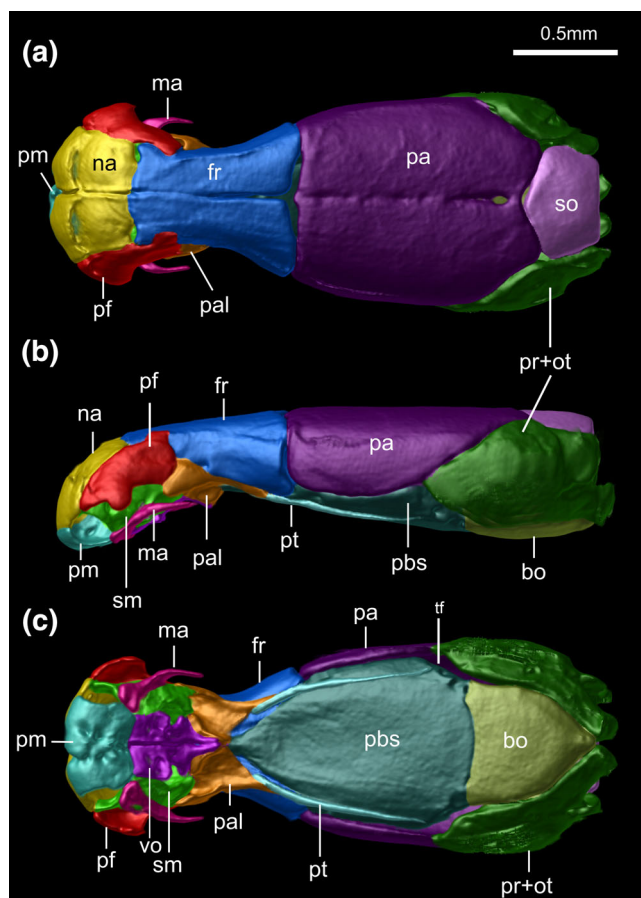
FIGURE 8 Three-dimensional reconstruction of the skull and cervical vertebrae of *Tetracheilostoma* spp. in anterior (a,e,i,m), dorsal (b,f,j,n), lateral (c,g,k,o), and ventral (D,H,L,P) views. (A–D) Paratype of *T. carlae* (BMNH 1969.792); (E–H) *T. bilineata* (USNM 564808); (I–L) *T. bilineata* (ZMB 4116); (M–P) *T. bilineata* (ZMB 5056). Scales: 0.5 mm

the prefrontal might be present on the dorsal surface of each element in *T. bilineata* ($n = 2$; Figure 8n). The lateral surface of the frontal surrounds the anteriorly oriented optic nerve foramen (Figures 1b, 6b,d, 8c,g,k,o, and 9b). The frontals meet medially (internally) and dorsal to the parabasisphenoid, forming the wide frontal subolfactory processes (Figures 3b and 11b).

The *parietal* (Figures 1–3, 6, and 8–11) represents a single (fused) unit, even though in one specimen of *M. leptepileptus* (Figure 9a) a medial and incomplete sulcus seems to separate this bone in two halves. In *Tetracheilostoma*, it is also fused to the supraoccipitals posteriorly (Figures 1, 6, and 8). This element comprises about one-half the length of the entire skull, being slightly longer than wide, without any trace of a dorsal fontanelle (Figures 1–3, 6, and 8–11). In both genera, the parietal contacts the frontals anteriorly, the supraoccipital posteriorly (in *Mitophis*), the fused prootics + otooccipitals posteriorly, and the parabasisphenoid ventrally (Figures 1 and 9). However, the posterior contact of the parietal with the
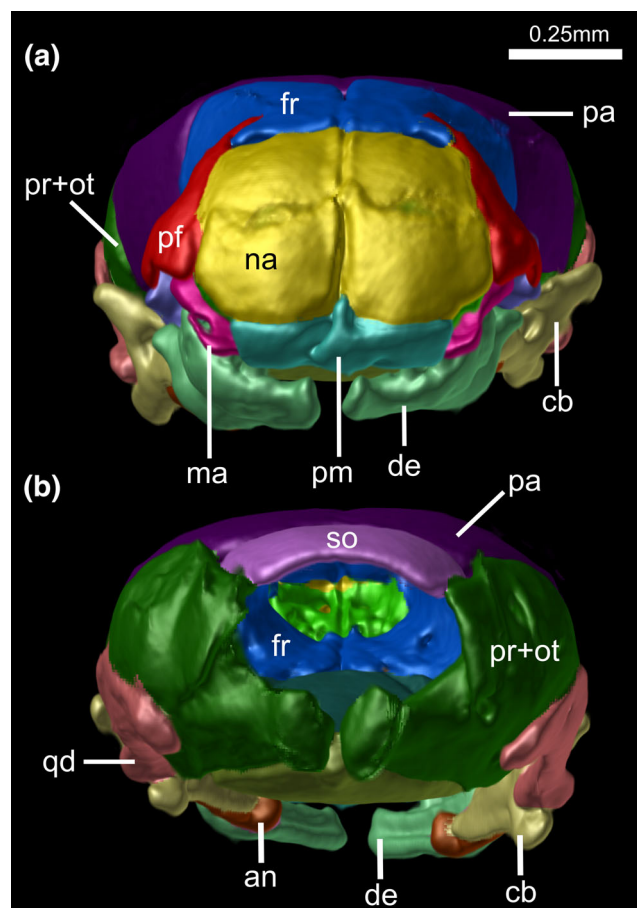
fused prootics + otooccipitals is distinct between *Tetracheilostoma* and *Mitophis*. While in *Tetracheilostoma* the parietal bends medially to form an internal pillar that ventrally contacts the clinoid process of the parabasisphenoid, and is limited posteriorly by the prootics + otooccipitals (Figure 3b), in *Mitophis* the parietal does not bend medially (i.e., an internal pillar is absent), fitting medially to the fused prootics + otooccipitals (Figure 11b). Therefore, in *Mitophis* the parietal is not limited posteriorly to the anterior portion of the prootics + otooccipitals. Dorsally, the medial anterior limit that contacts the frontals projects into a tapered process that separates both frontals in their posterior limit (inconspicuous in *M. leptepileptus*; Figures 1a, 6e, 8b,f,j,n, and 9a). The lateral walls of the parietal are convex (Figures 1b and 9b), and in *Mitophis*, the dorsoposterior contact with the supraoccipital occurs through a concave suture (Figure 9a), while in *Tetracheilostoma* it gradually tapers posteriorly to end in a convex suture with the prootics + otooccipitals (Figures 1a and 8b,f,j,n). The parietal descends comprising the lateral

FIGURE 9 Dorsal (a), lateral (b), and ventral (c) views of the three-dimensional reconstruction of the skull of *Mitophis leptepileptus* (USNM 576217) based on μCT data. Different skull elements are digitally colored to improve visualization of elements, and the mandibles and quadrates were digitally removed for better visualization. Abbreviations are as follows: bo, basioccipital; fr, frontal; ma, maxilla; na, nasal; pa, parietal; pal, palatine; pbs, parabasisphenoid; pf, prefrontal; pm, premaxilla; pr + ot, fused prootic + otooccipital; pt, pterygoid; sm, septomaxilla; so, supraoccipital; tf, trigeminal nerve foramen; vo, vomer

FIGURE 10 Anterior (a) and posterior (b) views of the three-dimensional reconstruction of the skull and lower jaw (suspensorium + mandible) of *Mitophis leptepileptus* (USNM 576217) based on μCT data. Different skull elements are digitally colored to improve visualization of elements. Abbreviations are as follows: an, angular; cb, compound bone; de, dentary; fr, frontal; ma, maxilla; na, nasal; pa, parietal; pf, prefrontal; pm, premaxilla; pr + ot, fused prootic+otooccipital; qd, quadrate; so, supraoccipital

limit of the trigeminal nerve foramen, which is formed exclusively with the fused prootic + otooccipital in *Tetracheilostoma* (Figure 1b), while in *M. leptepileptus* it is also formed by the parabasisphenoid (Figure 9b).

The *parabasisphenoid complex* (Figures 1, 3, 7–9, and 11) is a roughly triangular bone that forms the majority of the basicranium, being extremely tapered anteriorly. It is located dorsally to the vomers and palatines, and ventrally to the frontal subolfactory processes, broadly contacting the anterior margin of the basioccipital posteriorly, and the frontals, the parietal and the fused prootics + otooccipitals laterally. Its posterior suture with the basioccipital (Figures 1c, 8d,h,l,p, and 9c) is slightly convex. In *Tetracheilostoma*, a small foramen is formed on each side with the fused prootic + otooccipital,

opening internally into the wide trigeminal nerve foramen (*n* = 3). The clinoid process—present exclusively in *Tetracheilostoma*—represents an osseous projection that fits dorsally to the parietal pillar (Figures 3a,b and 7a). The parabasisphenoid is perforated by two pairs of foramina in its dorsal (internal) lamina: (a) the pair of internal carotid openings (located more posteriorly), and (b) the abducens nerve (VI) foramen (located more anteriorly); both located posterior to the clinoid process in *Tetracheilostoma* (Figures 3b and 11b). In two individuals of *T. bilineata*, the pair of internal carotid foramina are indistinct or absent; while in *T. carlae* only the posterior pair (internal carotid foramina) are distinct. In *M. leptepileptus,* an additional pair of anterolateral foramina pierce the parabasisphenoid dorsal lamina, and might
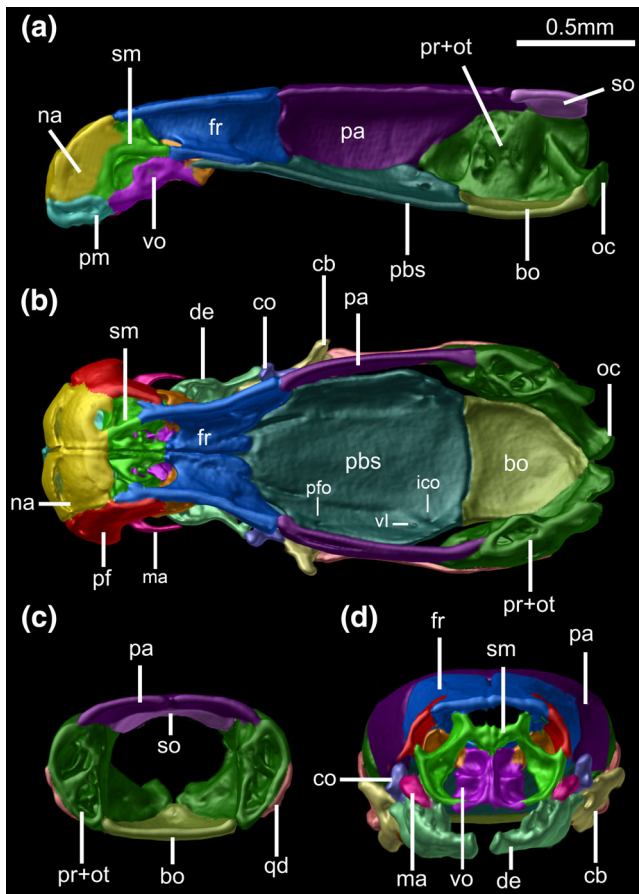
FIGURE 11 Three-dimensional cutaway views along the sagittal (a), vertical (b), and transverse (c,d) axes of the skull of *Mitophis leptepileptus* (USNM 576217) based on μCT data. Different skull elements are digitally colored to improve visualization of elements. Abbreviations are as follows: bo, basioccipital; cb, compound bone; co, coronoid; de, dentary; fr, frontal; ico, internal carotid opening; ma, maxilla; na, nasal; oc, occipital condyle; pa, parietal; pbs, parabasisphenoid; pf, prefrontal; pfo, palatine branch of the facial nerve opening; pm, premaxilla; pr + ot, fused prootic +otooccipital; qd, quadrate; sm, septomaxilla; so, supraoccipital; vI, abducens nerve (VI) foramen; vo, vomer

represent the opening for the palatine branch of the facial nerve foramen (Figure 11b).

The *basioccipital* (Figures 1–3 and 7–11) is a flat and subtriangular plate that broadly contacts the parabasisphenoid anteriorly and the fused prootics + otooccipitals laterally and posteriorly. In *Tetracheilostoma* the basioccipital is reduced, not covering a wide area of the posterior region of the basicranium (Figures 1c, and 8d,h,l,p), while in *M. leptepileptus* it is proportionally wider in comparison to *Tetracheilostoma* (Figure 9c). In ventral view (Figures 1c, 8d,h,l,p, and 9c), it is wide at its anterior suture with the parabasisphenoid, gradually tapering posteriorly until fitting medially to the ventroposterior portion of the fused

prootics + otooccipitals that meet medially. Therefore, the basioccipital does not participate in the formation of the foramen magnum in either genus.

The *supraoccipitals* (Figure 9a) are fused into a single pentagonal plate in *Mitophis*. As mentioned in the descriptive section of "parietal," the supraoccipitals are indistinct and most likely fused to the parietal in *Tetracheilostoma*, and therefore will not be described herein. In *Mitophis*, the supraoccipital broadly contacts the parietal anteriorly and the prootics + otooccipitals laterally. This element participates in the formation of the dorsal area of the foramen magnum (Figure 10b). It does not participate in any of the otic capsule internal walls (Figure 11) and is not involved in the formation of the osseous labyrinth. This condition—that is, absence of participation of the supraoccipital in the formation of the osseous labyrinth—is also evident from the supraoccipital component of the parietal in *Tetracheilostoma* (Figure 3).

The fused *prootic + otooccipital* (Figures 1–3, 6, and 8–11) is paired, represented by a wide convex plate that encloses the dorsal, medial, lateral and posterior walls of the *otic capsule*. Both of these fused elements provide the whole posterolateral cover of the skull, also enclosing the entire circumference of the foramen magnum in *Tetracheilostoma* (Figure 2b). They are in broad contact with the parietal anteriorly, the parabasisphenoid anteroventrally and the basioccipital ventroposteriorly. While in *Tetracheilostoma* (except one specimen of *T. bilineata*; Figure 8l) the occipital condyle contacts its counterpart medially, in *M. leptepileptus* these condyles are not in contact medially (Figures 9c, and 10b). The medial (internal) wall of each fused prootic + otooccipital is poorly ossified and pierced by a pair of acoustic nerve foramina (Figure 6L). In *Tetracheilostoma*, the wide ellipsoidal medial aperture of the *recessus scalae tympani* pierces the medial lamina of the prootic + otooccipital (Figure 6l). A statolithic mass in the *cavum vestibuli* is absent in all *Tetracheilostoma* individuals and *M. leptepileptus* (Figures 3b,c and 11b,c). The posterior surface (external) is perforated by the vagus nerve foramen that opens internally in the braincase (Figure 6n); this foramen is indistinct in the right element of *Mitophis*. The moderately expanded stapedial footplate lies within the *fenestra vestibuli*, not being co-ossified to this cavity. In one specimen of *T. bilineata* the footplate is indistinct. The short, ossified portion of the stapedial shaft emerges from the posterior portion of the stapedial footplate, extending in a posterolateral direction through a small opening of the lateral lamina of the prootic + otooccipital into the space between the otic capsule and the quadrate (Figure 6N).

3.2 | Lower jaw morphology of *Mitophis* and *Tetracheilostoma*

The lower jaw is suspended from the skull by a pair of quadrates, which are connected to the skull by a series of muscles, ligaments, and cartilages (Kley, 2006; Martins, Passos, & Pinto, 2019). The quadrate is slightly shorter than the mandible in all specimens analyzed.

The *quadrate* (Figures 3, 8–10, and 12–15) lies adjacent to the ventral aspect of the otic capsule, distally articulating with the lower jaw and forming the quadratomandibular joint. The quadrate is wide and laterally compressed at the articulation with the otic region, bearing a ventroposterior process that is anteriorly perforated by a small foramen (although it might vary bilaterally or even may be absent in one side of *T. bilineata*, n = 1). In *M. leptepileptus*, the posterior process is long and conspicuous (Figures 14 and 15). A stapedial cartilage was indistinct in the analyzed cleared and stained specimen of *M. leptepileptus*. The quadrate distally twists along its own axis, becoming progressively more slender and angling medially toward its distal head, the latter being covered by cartilage. A foramen at the dorsoanterior face of the quadrate is most likely indistinct/absent in most analyzed specimens/species, except for one specimen of *T. bilineata* and the only individual of *T. carlae*, which seems to exhibit a concavity at this region that might represent a foramen. In *M. leptepileptus* the anterior foramen is present and wide in one of the specimens analyzed (Figure 15b).

The *mandibles* (Figures 2, 3, 8, 10, and 12–15) are subterminal and composed of the dentaries, the splenials, the angulars, the coronoids, and the compound bones. Each *dentary* is composed of four distinguishable regions (sensu Kley, 2006; see Figures 12–15): (a) dental concha, (b) symphyseal process, (c) body of the dentary, and (d) dorsoposterior process. The dental concha comprises the largest portion of the dentary, resembling a shallow ellipsoidal bowl with prominent convex surface in lateral view (Figures 12–15). *Tetracheilostoma* spp. exhibit a series of four (n = 1, *T. carlae*) or five (n = 4, *T. bilineata*) slightly medially curved and long teeth with pleurodont implantation, lacking a medial (lingual) bony support, while *Mitophis* exhibits a series of four teeth. The symphyseal process of the dentary corresponds to a reduced anteromedial projection of the body of the dentary, projecting beyond the anterior margin of the dental concha (Figures 12–15). Ventral to the dental concha, the body of the dentary represents a basal portion of the dentary (Figures 12–15). Its dorsomedial margin is notched by Meckel's groove, which extends toward the ventral region of the medial surface of the dentary, being open throughout most of its extent (Figures 12a,c,13b,d,f,h,
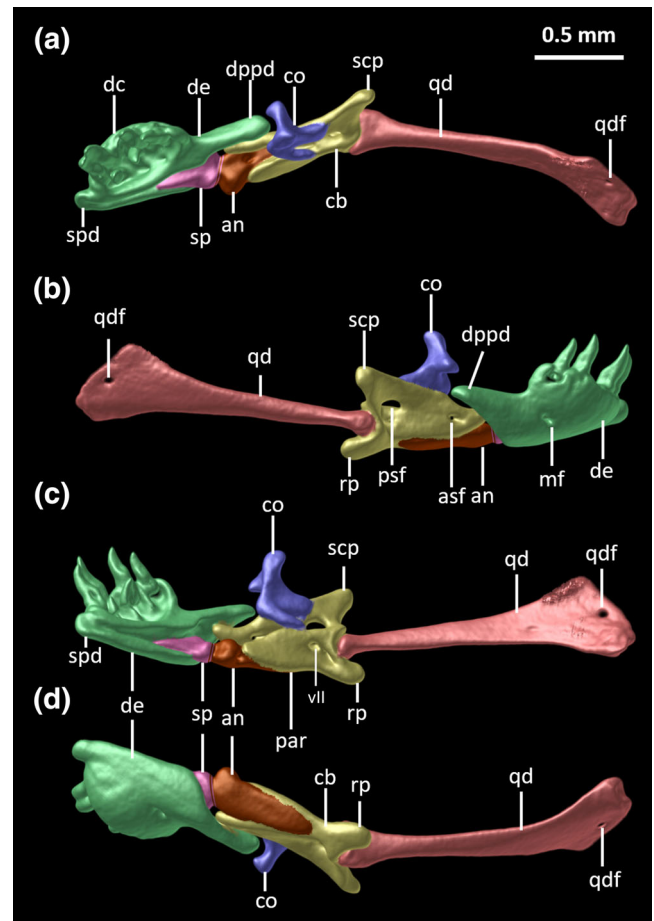
FIGURE 12 Dorsal (a), lateral (b), medial (c), and ventral (d) views of the three-dimensional reconstruction of the suspensorium (quadrate + lower jaw) of *Tetracheilostoma bilineata* (BMNH 1853.2.4.36) based on μCT data. Different elements are digitally colored to improve visualization of elements. Abbreviations are as follows: an, angular; asf, anterior surangular foramen; cb, compound bone; co, coronoid; dc, dental concha; de, dentary; dppd, dorsoposterior process of dentary; mf, mental foramen; par, prearticular lamina of compound bone; psf, posterior surangular foramen; qd, quadrate; qdf, quadrate foramen; rp, retroarticular process; scp, supracotylar process of surangular; sp, splenial; spd, symphyseal process of dentary; vII, facial nerve foramen

and 14a,c). In *M. leptepileptus*, the Meckel's cartilage extends from the posterior limit of the symphyseal process until ½ the length of the posterior surangular foramen of the compound bone (Figure 15B). A reduced mental foramen is located at the lateral surface of the body of the dentary and below the level of the last tooth (Figures 12b, 13, 14b, and 15a). The posteromedial portion of the body of the dentary supports the anterior process of the splenial (Figures 12a,c, 13, 14a,c, and 15b), covering it almost completely in lateral view. The dorsoposterior process of dentary is long in *Tetracheilostoma*, exceeding the anterior limit of the coronoid (Figures 12
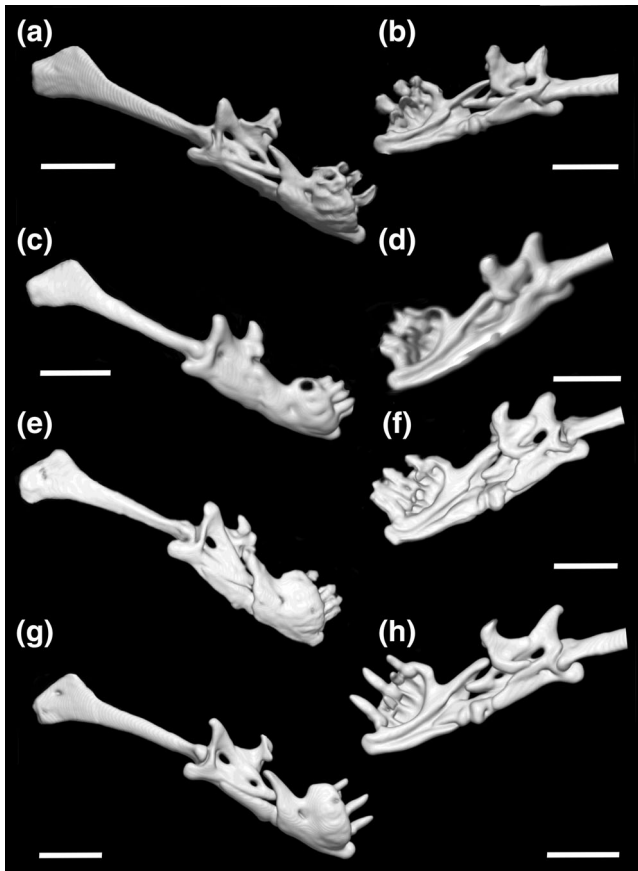
FIGURE 13 Lateral (a,c,e,g) and medial (b,d,f,h) views of the three-dimensional reconstruction of the suspensorium (quadrate + lower jaw) of *Tetracheilostoma* spp. based on μCT data. Figures in medial view had their quadrate digitally cut to improve visualization. (a,b) Paratype of *T. carlae* (BMNH 1969.792); (c,d) *T. bilineata* (USNM 564808); (e,f) *T. bilineata* (ZMB 4116); (g,h) *T. bilineata* (ZMB 5056). Scales: 0.5 mm

FIGURE 14 Dorsal (a), lateral (b), medial (c), and ventral (d) views of the three-dimensional reconstruction of the suspensorium (quadrate + lower jaw) of *Mitophis leptepileptus* (USNM 576217) based on μCT data. Different elements are digitally colored to improve visualization of elements. Abbreviations are as follows: an, angular; asf, anterior surangular foramen; cb, compound bone; co, coronoid; dc, dental concha; de, dentary; dppd, dorsoposterior process of dentary; mf, mental foramen; par, prearticular lamina of compound bone; psf, posterior surangular foramen; qd, quadrate; qdf, quadrate foramen; rp, retroarticular process; scp, supracotylar process of surangular; sp, splenial; spd, symphyseal process of dentary; vII, facial nerve foramen
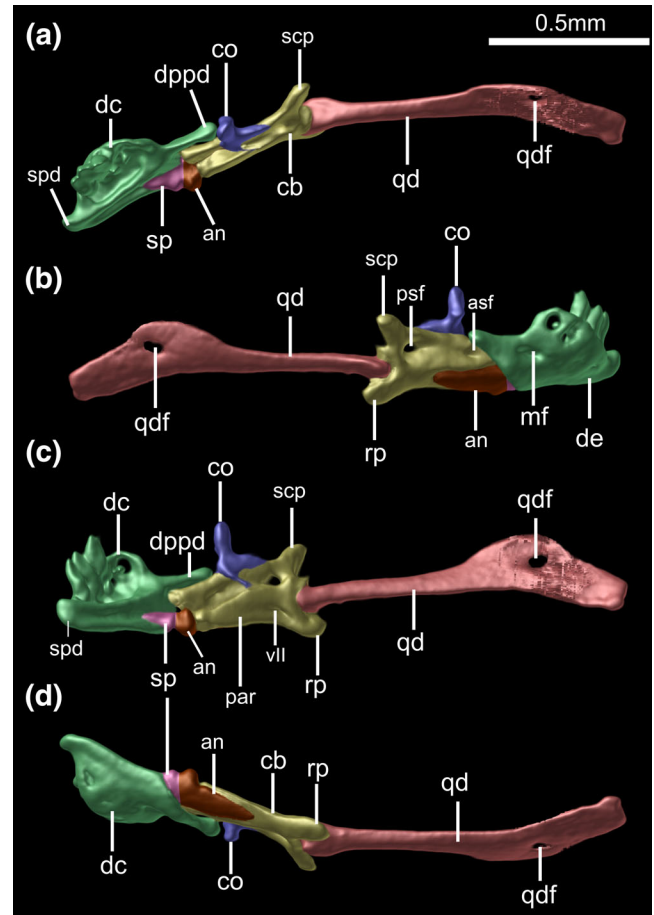
and 13); but is short and stout in *M. leptepileptus*, not reaching the anterior limit of the coronoid (Figures 14 and 15).

The *splenial* (Figures 12–15) is the smallest bone in the lower jaw, being approximately conical in shape and medially abutting via a tight syndesmosis (Kley, 2006) to the concave area of the body of the dentary. In *M. leptepileptus*, the splenial is short, triangular and approximately as long as high in one specimen (Figure 15b), and slightly longer than wide in the other (Figure 14c). It articulates with the angular posteriorly through a concave posterior surface (=condylar head of splenial), thus forming a relevant portion of the highly kinetic intramandibular joint. It tapers anteriorly reaching the level of the fourth ($n = 3$) or fifth tooth ($n = 1$) in *T. bilineata*; the fourth tooth in *T. carlae*; and the last (fourth) in *M. leptepileptus*. An anterior mylohyoid foramen is absent.

The *angular* (Figures 12–15) is also conical, resembling the splenial in shape, although it is stouter than the former. The cotylar head of the angular is larger than the splenial condylar head, being slightly convex (Figures 12a,c, 13b,d,f,h, and 14a,c). The angular body posterior to the cotylar head is laterally compressed, fitting laterally to the prearticular lamina of the compound bone. In medial view, the prearticular lamina of the compound bone covers the posterior process of the angular; therefore, only the cotylar head of the angular is significantly exposed in this view. The posterior mylohyoid foramen (indistinct in *Mitophis*) is located on the ventral surface of the angular bone, posterior to the
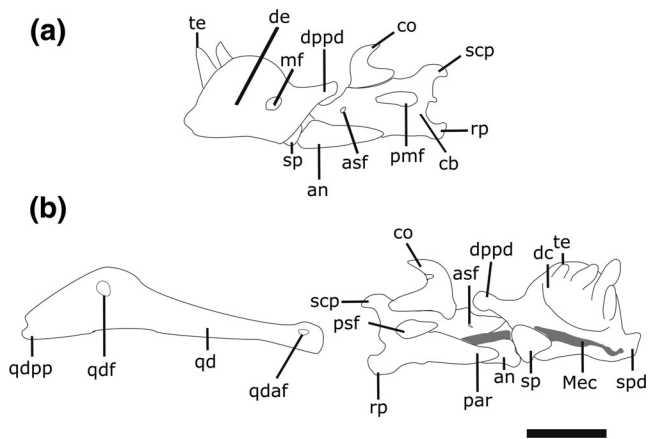
FIGURE 15 Schematic illustration of the lower jaw of *Mitophis leptepileptus* (KU 275558) in lateral (a) and medial (b) views. Abbreviations are as follows: an, angular; asf, anterior surangular foramen; cb, compound bone; co, coronoid; dc, dental concha; de, dentary; dppd, dorsoposterior process of dentary; Mec, Meckelian cartilage; mf, mental foramen; par, prearticular lamina of compound bone; psf, posterior surangular foramen; qd, quadrate; qdaf, quadrate anterior foramen; qdf, quadrate foramen; qdpp, quadrate posterior process; rp, retroarticular process; scp, supracotylar process of surangular; sp, splenial; spd, symphyseal process of dentary; te, teeth. Scale 0.5 mm

enlarged cotylar head of the angular. The angular tapers posteriorly, reaching the level of the posterior surangular foramen (Figures 12d, 13a,c,e,g, and 14b).

The *compound bone* (Figures 12–15) represents the fusion of the articular, prearticular, and surangular into a single unit. The surangular and prearticular components of the compound bone are distinguishable by a medial separation throughout their medial contact, both fused to the articular posteriorly, with the surangular representing the widest region of the compound bone (Figures 12–15). The surangular lamina is located laterally on the compound bone, being triangular in shape and tapering anteriorly toward the dorsoposterior process of the dentary, being slightly occluded by the latter in lateral view (Figures 12b,13a,c,e,g, and 14b). This lamina is pierced by a reduced anterior (indistinct in one specimen of *Tetracheilostoma*) and a wide posterior foramen, with its dorsal lamina supporting the coronoid (Figures 12b and 14a). The prearticular lamina of the compound bone is medially located, long, slightly tapering anteriorly, with a convex anterior margin (Figures 12c, 13b,d,f,h, and 14c). Its dorsoanterior portion receives the ventral processes of the coronoid, while its posteromedial lamina is pierced by the conspicuous *chorda tympani* of the hyomandibular ramus of the facial nerve (VII; Figures 12 and 14). The articular region of the compound bone projects dorsally, exhibiting a wide posterior concavity that forms the articular cotyle from the quadratomandibular joint (Figures 12–15). The retroarticular process represents a short posteroventral elongation of the articular lamina (Figures 12–15). The supracotylar process is concave posteriorly, projecting posteriorly, although in one specimen of *M. leptepileptus* it projects into a claw-like process (Figure 15).

The *coronoid* (Figures 12–15) is complex in shape, located dorsomedially to the compound bone, consisting of an anteroposteriorly compressed dorsal process, a midposterior and triangular surangular process, and a ventromedial and laterally compressed prearticular process. Its dorsal process is bifurcated in *Tetracheilostoma*, projecting into a medial and a lateral stout process; the lateral slightly bending ventrally, while the medial bends dorsoposteriorly (Figures 12–13). In *Mitophis*, this process is bifurcated ($n = 1$; Figure 14) or trifurcated (Figure 15), with—besides the lateral and medial processes—a short dorsal process. The anterior lamina of the coronoid is conspicuously concave (Figures 12a,c, and 14c). The surangular process of the coronoid is a wide ellipsoidal process that abuts dorsomedially the surangular; while the prearticular process of the coronoid is reduced and ellipsoidal and is laterally compressed and oblique (Figures 12–15).

3.3 | Postcranial osteology of *Mitophis* and *Tetracheilostoma*

Herein we describe the cervical (atlas and axis), trunk, cloacal and caudal vertebrae morphology of *Mitophis* and *Tetracheilostoma* and provide quantitative data for the trunk, cloacal, and caudal vertebrae. In both genera, the rudimentary pelvic elements seem to be absent (except in *M. calypso*), but in one cleared and stained specimen of *M. leptepileptus*, a very small rod-like cartilaginous element seems to be present at the cloacal region.

3.3.1 | Cervical vertebrae morphology

The *atlas* (Figures 16a–e and 17a–e) is composed of the paired neural arches, lacking a neural spine, ribs, and ventral intercentrum I. The neural arches are dorsoventrally flattened elements that are in contact with each other dorsally and ventrally and surround the semicircular neural canal. Each neural arch expands anteriorly and posteriorly in its dorsal region, also enlarging midventrally to form articular facets, which are covered by cartilage and articulate with the occipital condyle of the skull. Each neural arch also bears short lateral transversal processes. In one specimen of *T. bilineata* the right neural arch is dorsolaterally pierced by a foramen.
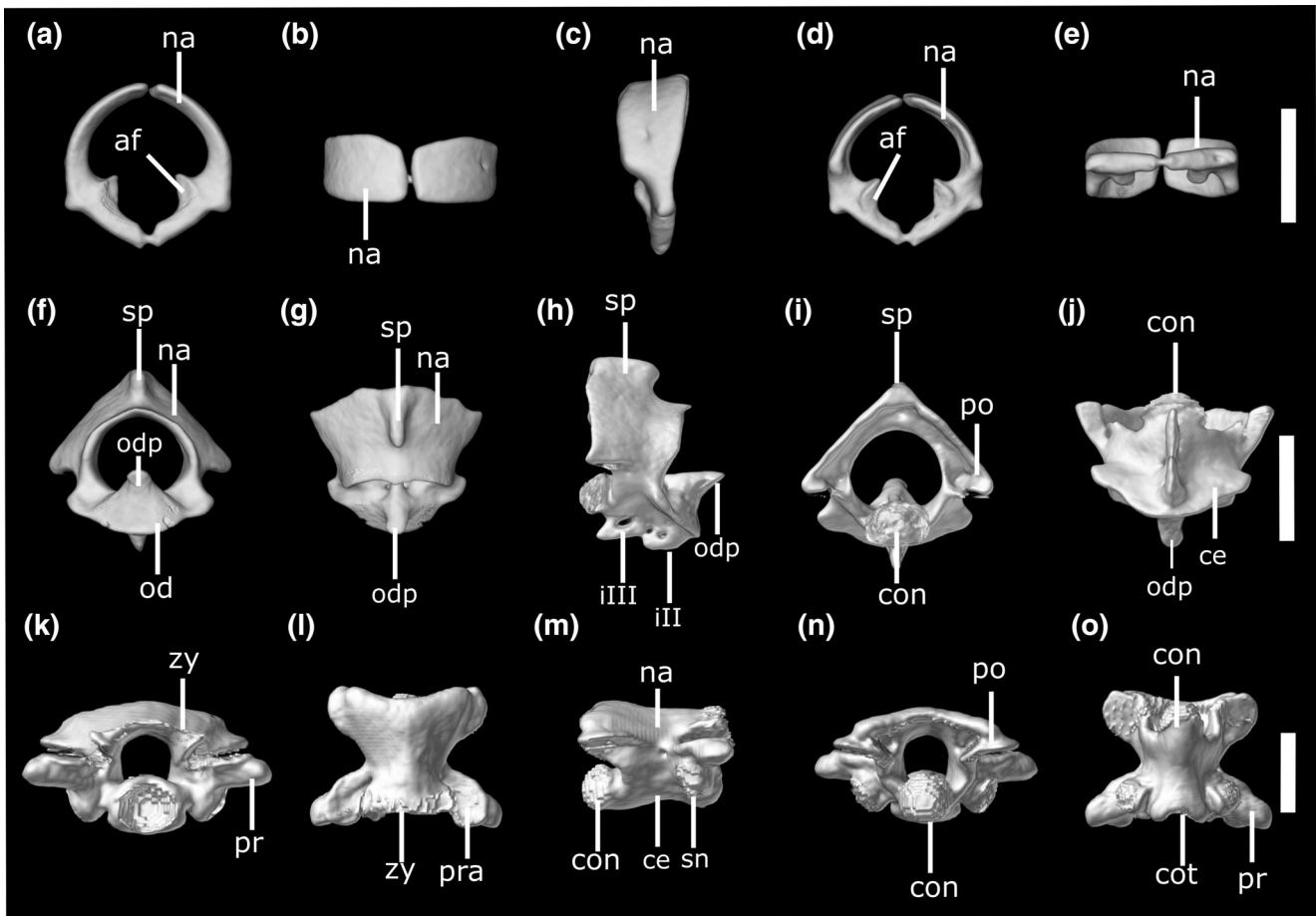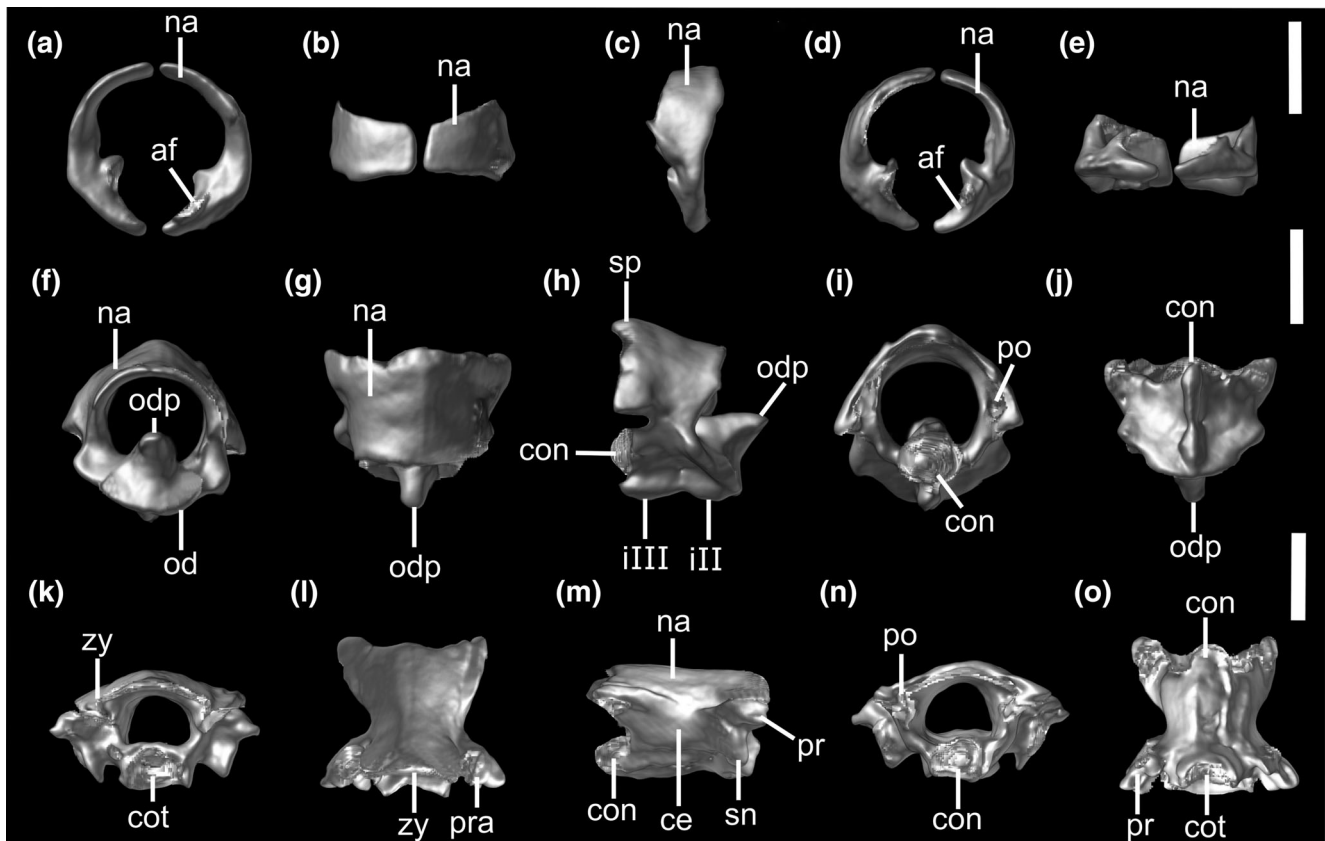
FIGURE 16 Three-dimensional reconstruction of the atlas (a–e), axis (f–j), and midtrunk (k–o) vertebra of *Tetracheilostoma bilineata* (BMNH 1853.2.4.36) in anterior (a,f,k), dorsal (b,g,l), lateral (c,h,m), posterior (d,i,n), and ventral (e,j,o) views. Abbreviations are as follows: af, articular facet; ce, centrum; con, condyle; cot, cotyle; iII, intercentrum II; iIII, intercentrum III; na, neural arches; od, odontoid; odp, odontoid process; po, postzygapophysis; pr, prezygapophysis; pra, prezygapophyseal articular facet; sn, synapophyses; sp, spinal process; zy, zygosphene. Scales: 0.5 mm

The *axis* (Figures 16f–j and 17f–j) is composed of a centrum, moderate neural arches, a moderately-developed spinal process, an odontoid process, a dorsoanterior process of the odontoid, a pair of undeveloped transverse processes, postzygapophyseal articular facets, a condyle and the intercentra II and III, which are very reduced in *Mitophis*. As with the atlas, this vertebra has no vestiges of ribs. In *Tetracheilostoma*, the axis spinal process is represented by an elevated dorsal keel that extends through almost all the middorsal portion of the axis, except its anteriormost extent (Figure 16h). In *Mitophis*, however, the axis spinal process is very reduced and represented by a dorsal process at the posterodorsal surface of this element (Figure 17h). The neural canal is approximately rounded, and the odontoid is an osseous process attached to the anteroventral surface of the neural arches (Figures 16f–h and 17f–h). A dorsoanterior projection from the odontoid is visible anteriorly, slightly tapering anteriorly and ending in a rounded distal (= anterior) limit

(Figures 16f–h and 17f–h). A well-developed (*Tetracheilostoma*) keel extends over the ventral lamina of the neural canal until reaching the condyle posteriorly. No foramina are distinct in the axis centrum. The transverse processes are reduced and emerge from the surface portion of the centrum. They are transversely oriented, rod-shaped, and convex at their dorsal portion. The intercentra II and III are laterally compressed, fused and pointed ($n = 1$, *Tetracheilostoma*, Figure 16h; *M. leptepileptus*, $n = 1$, Figure 17) or keel-shaped ($n = 2$, *Tetracheilostoma*; $n = 1$, *M. leptepileptus*; sensu Holman, 2000).

3.3.2 | Trunk, cloacal, and caudal vertebrae

The species of *Tetracheilostoma* herein examined quantitatively for vertebral data (i.e., *T. bilineata*, *T. breuili*, and *T. carlae*) exhibit a total of 152–167 trunk vertebrae, 3–4 cloacal vertebrae and 15–16 caudal vertebrae (Table 1).

FIGURE 17 Three-dimensional reconstruction of the atlas (a–e), axis (f–j), and midtrunk (k–o) vertebra of *Mitophis leptepileptus* (USNM 576217) in anterior (a,f,k), dorsal (b,g,l), lateral (c,h,m), posterior (d,i,n), and ventral (e,j,o) views. Abbreviations are as follows: af, articular facet; ce, centrum; con, condyle; cot, cotyle; iII, intercentrum II; iIII, intercentrum III; na, neural arches; od, odontoid; odp, odontoid process; po, postzygapophysis; pr, prezygapophysis; pra, prezygapophyseal articular facet; sn, synapophyses; sp, spinal process; zy, zygosphene. Scales: 0.25 mm

TABLE 1 Quantitative data for the number of trunk, cloacal, and caudal vertebrae of *Mitophis* and *Tetracheilostoma* based on X-rayed and cleared and stained specimens

	Total number of trunk vertebrae	Total number of cloacal vertebrae	Total number of caudal vertebrae
Mitophis asbolepis	279(1)	?	?
Mitophis calypso	351 ± 1, 350–352(2)	?	?
Mitophis leptepileptus	377.7 ± 12.6, 354–391(7)	6(1)	20 ± 1.4, 19–21(2)
Mitophis pyrites	259.5 ± 0.7, 259–260(2)	?	?
Tetracheilostoma bilineata	155 ± 4.3, 152–160(2)	3(1)	16(1)
Tetracheilostoma breuili	159.5 ± 2.2, 155–162(8)	3(1)	16(1)
Tetracheilostoma carlae	166 ± 1.4, 165–167(2)	3.5 ± 0.7, 3–4(2)	15.5 ± 0.7, 15–16(2)

Note: For species with sample number >1, formula indicates "Mean ± standard deviation, Min–Max, (sample size)." The symbol "?" means that such data was not accessible.

The species of *Mitophis* herein examined (i.e., *M. asbolepis*, *M. calypso*, *M. leptepileptus*, and *M. pyrites*) exhibit a total of 259–391 trunk vertebrae, 6 cloacal vertebrae (based only on *M. leptepileptus*) and 19–21 caudal vertebrae (based only on *M. leptepileptus*; Table 1).

The first *trunk vertebrae* do not bear conspicuous zygosphenes, which are gradually perceptible posteriorly from the posterior 1/3 of the vertebral column. The midtrunk vertebrae (Figures 16k–o and 17k–o) bear the anterior limit of the zygosphene convex with tapered

lateral limits that curve medially. The prezygapophyses are visible in anterior view and represent lateral projections that bear prezygapophyseal articular facets that are oval or ellipsoidal (Figures 16l and 17l). The prezygapophyseal accessory processes are quadrangular and truncate (Figures 16k and 17k). The cotyle is a wide oval and concave articular surface located anterior to the centrum, with absent/indistinct paracotylar foramina (Figures 16k and 17k). The vertebral centrum is narrow, with the synapophyses emerging laterally at its anteroventral region (Figures 16m, and 17m). The synapophyses form a single facet without any clear distinction between the diapophyseal and parapophyseal areas (Figures 16m and 17m). The lateral foramina and haemal keel are absent, and a subcentral foramen is absent. In the posterior region of the trunk vertebrae, the zygantrum forms the posterior roof for the neural canal. The zygantral articular facets are V-shaped and present in the internal lateral limit of the neural canal. The postzygapophyses are short and triangular and laterally emerge from the neural arch (Figures 16n and 17n). The condyle is wide, oval and articulates with the cotyle of the subsequent vertebrae (Figures 16n and 17n). The *cloacal vertebrae* (Figures 18 and 19) are compressed dorsoventrally when compared with the trunk vertebrae. Additionally, the cloacal vertebrae are particularly identifiable by the presence of paired lymphapophyses fused to their ventrolateral surfaces. The lymphapophyses develop ventrolaterally, with the dorsal element usually bending ventrally, while the ventral element bends dorsally. Each
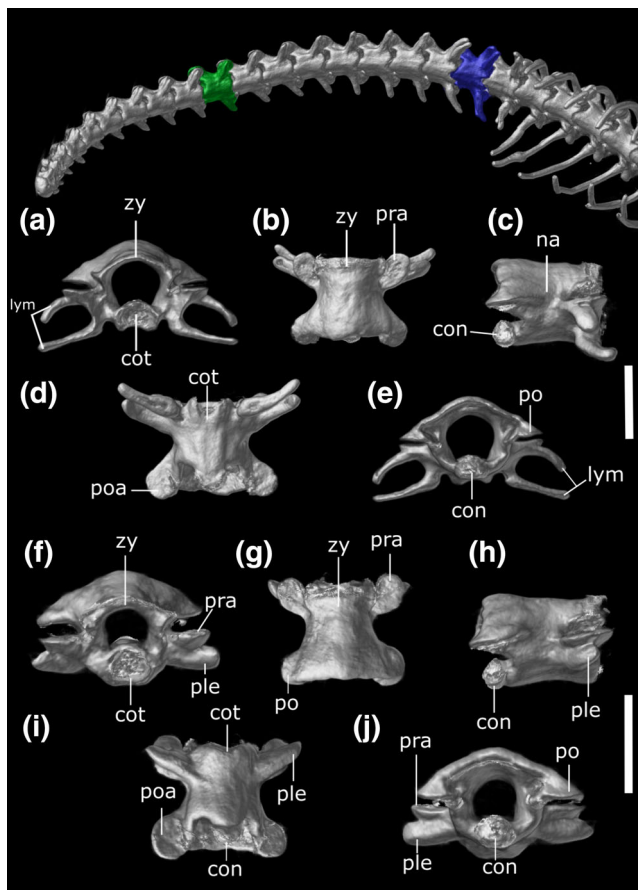
FIGURE 18 Three-dimensional reconstruction of the cloacal (a–e) and caudal (f–j) vertebra of the syntype of *Tetracheilostoma bilineata* (MNHN 1994.1147) in anterior (a,f), dorsal (b,g), lateral (c,h), ventral (d,i), and posterior (e,j) views. The figure above vertebrae a–j represents a dorsal view of the posterior region of the body indicating the cloacal (blue) and caudal (green) vertebra isolated and illustrated. Abbreviations are as follows: con, condyle; cot, cotyle; lym, lymphapophyses; na, neural arches; ple, pleurapophyses; po, postzygapophysis; poa, postzygapophyseal articular facet; pra, prezygapophyseal articular facet; zy, zygosphene. Scales: 0.5 mm
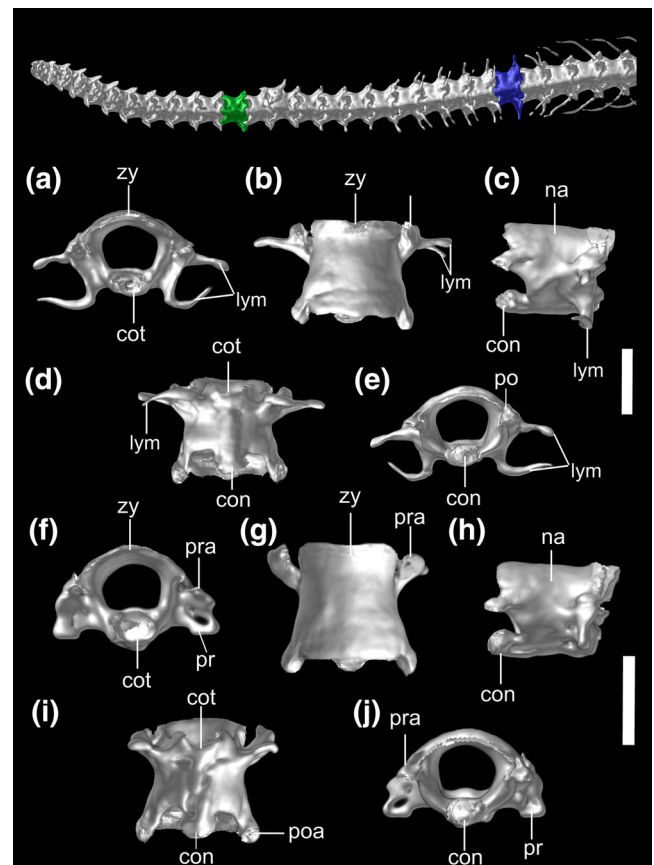
FIGURE 19 Three-dimensional reconstruction of the cloacal (a–e) and caudal (F–J) vertebra of *Mitophis leptepileptus* (USNM 576217) in anterior (a,f), dorsal (b,g), lateral (c,h), ventral (d,i), and posterior (e,j) views. The figure above vertebrae a–j represents a dorsal view of the posterior region of the body indicating the cloacal (blue) and caudal (green) vertebra isolated and illustrated. Abbreviations are as follows: con, condyle; cot, cotyle; lym, lymphapophyses; na, neural arches; po, postzygapophysis; poa, postzygapophyseal articular facet; pr, prezygapophysis; pra, prezygapophyseal articular facet; zy, zygosphene. Scales: 0.25 mm

lymphapophysis bears a short and tapered costal cartilage at its distal tip. A short prezygapophyseal accessory process is also present, while the synapophyses, the interzygapophyseal keel, the subcentral keel, the haemal keel, and the subcotylar and paracotylar foramina are always absent. In comparison to the trunk vertebrae, the cloacal vertebrae bear moderate neural arches that develop anteriorly into a short zygosphene. Finally, the condyle of the cloacal vertebrae is considerably smaller than in the trunk vertebrae (Figures 18d and 19d). The *caudal vertebrae* (Figures 18f–j and 19f–j) resemble the cloacal vertebrae in shape except for the presence of paired pleurapophyses (vs. lymphapophyses in the cloacal vertebrae). However, in *M. leptepileptus*, the pleurapophyses seem to be totally absent, while in *Tetracheilostoma* they are very reduced (Figure 18). A haemapophysis, a lateral foramen, and paired subcentral foramina are absent. The prezygapophyseal articular facet is present (Figures 18g and 19g). The last two vertebrae are fused in *M. leptepileptus*.

3.4 | Visceral data for *Mitophis* and *Tetracheilostoma*

The *heart* (Figure 20a) is located at the midventral line of the body cavity, in 15% (% of snout-vent length) in *M. leptepileptus* and a mean of 22% in *T. bilineata*. The right atrium is long, about ½ heart total length and slightly shorter than the ventriculum. The posterior end of the left atrium lies more anteriorly than the right atrium. The posterior end of the ventriculum is slightly oriented to the right side of the body. The ventriculum is elongated and tapers at its posterior end, being approximately twice as long as the left atrium and slightly longer than the right atrium in *M. leptepileptus*, but about the same size as the right atrium in *T. bilineata*.

The *thyroid gland* (Figure 20a) is short, anterior to the heart, with a slight gap from the heart. Lateral to the thyroid gland, a single pair of *thymus glands* are located at both sides of the thyroid, being ellipsoidal and reduced (<1% of the SVL). The right thymus is slightly longer than the left, with its middle point slightly more anterior than the left one. Both thymi are in contact with the thyroid gland.

A *tracheal lung* and a *left lung* are absent. The *cardiac lung* is unicameral, with adjacent foramina. The *right lung* is long, unicameral, bearing faviform parenchyma organized in two layers more anteriorly (sensu Wallach, 1998a, 1998b), while its posterior portion is typically trabecular. The right lung extends posteriorly to constitute about 22% of the SVL in *T. bilineata*, with a posterior avascular folded region. The *right bronchus*
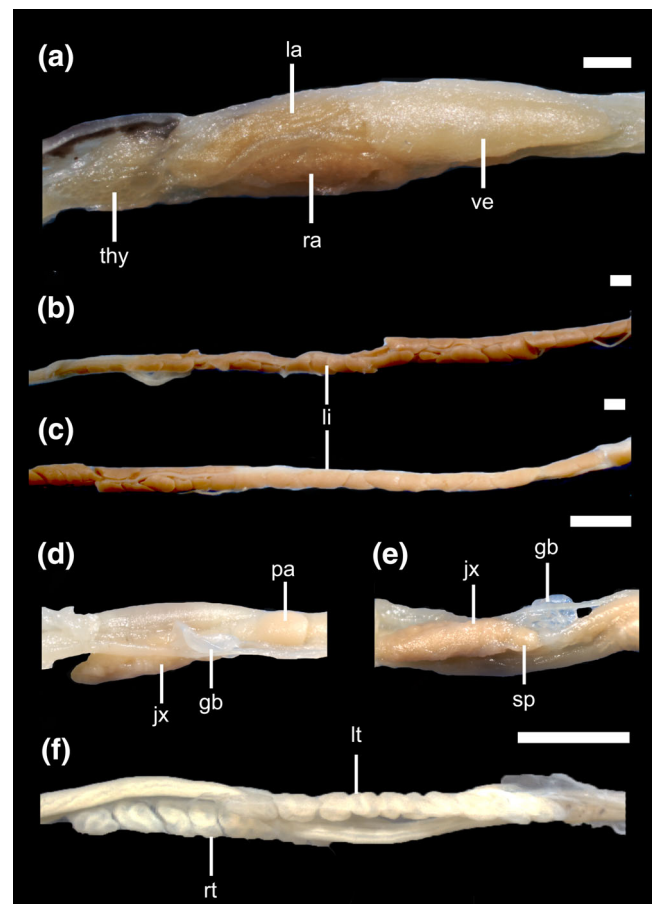
FIGURE 20 Photos of the viscera of *Mitophis leptepileptus* (KU 275548). Heart and thyroid gland (a); anterior half (b); and posterior half (c) of the liver; pancreas, gall bladder, spleen and juxtasplenic body of pancreas (d,e) and testicles (f). Abbreviations are as follows: gb, gall bladder; jx, juxtasplenic body of pancreas; la, left atrium; li, liver; lt, left testicle; pa, pancreas; ra, right atrium; rt, right testicle; sp, spleen; thy, thyroid gland; ve, ventriculum. Scale 1 mm

extends into the right lung, extending over more than 50% of its total length, with ring interspace becoming gradually wider and irregular toward its posterior portion.

The *liver* (Figure 20b,c) represents the longest organ in the body, extending over 34.6% (*M. leptepileptus*) and 41.2% (*T. bilineata*) of the SVL, located ventrally to the right lung. It is light brown in color (preserved specimen) and located on the right side of the body cavity, separated from the heart by a short gap (Table 2). This organ consists of two lobes (left and right) adjacent to the vena cava. Each lobe consists of a series of 54 (right lobe) and 28 (left lobe) segments in *Mitophis*, and 12 (right lobe) and 16 (left lobe) in *Tetracheilostoma*. In all specimens, the segments might exhibit a variable number of loops along their own axis. The anterior segments are usually longer than the posterior ones, with the anterior being

TABLE 2 Quantitative and qualitative data for the viscera of *Mitophis leptepileptus* and *Tetracheilostoma bilineata*

	M. leptepileptus (1♂)	*T. bilineata* (3♀)		*M. leptepileptus* (1♂)	*T. bilineata* (3♀)
HMP	15	22 ± 0.9 (21.3–22.7) 2	OM	—	79.7
AA	Left	Left	RTM	78.8	—
LAL	38.5	32.5 ± 1.9(31–33.7)2	LTM	81.2	—
RAL	42.5	47.8 ± 2.8(46–50)2	RTL	4	—
VL	58.4	47.7 ± 5.7(43.6–51.7)2	LTL	2.6	—
HLG	7.7	6.94	SRT	9	—
HLI	54.6	47.2	SLT	11	—
SHI	16.8	24.8	RAdM	?	79.4
RLL	41.2	25.3	LAdM	?	80
LLL	16.4	26.5	TAM	?	79.7
TLL	41.2	34.6	TKL	6.8	7.3 ± 1.4 (5.8–8.6) 3
RLM	46.1	50.8	TKM	74.9	85 ± 4.7 (79.7–88.5)3
LLM	35.3	48.3	KCG	8.5	9.4
AEL	Right	Right	KCI	25.1	13.2
ALA	3	3.9	GKG	0.8	2
PLA	21.7	4.8	RKM	85	86.4 ± 5.9 (79.6–90) 3
RL/LL	0.4	0.7	LKM	?	83.7 ± 3.5 (79.7–86.4)3
TRLS	54	16	LKL	3.7	4.1 ± 0.5 (3.6–4.4)3
TLLS	28	12	RKL	3.15	4.2 ± 0.3 (3.9–4.4)3
TLS	88	28	LA	0.35	0
LGG	2.9	0	RCL	0.7	0.95
LKG	19.4	15.4	TMP	9.3	13.8 ± 0.3 (13.5–14)2
KLI	66.6	54	RBL	?	17.5
LGI	44.4	36.9	PLRB	?	42.7
GBM	71.7	67.4	TLRB	?	40.6
GGG	9.5	8.5	TRBM	?	22.9
GKI	21.6	22.1	RLA	14.7	20.6 ± 1.5 (19.5–21.7)2
GbKG	16.9	13.2	RLP	?	47.4
TTS	20	-	RLuM	?	33.8
GTL	6.7	-	RLuL	?	22.2
TM	80	-			

Note: Values of organ size, midpoint, and gap are given as a % of the snout-vent length and follow Wallach (1998b). For species with sample number >1, formula indicates "Mean ± *SD*, (Min–Max), sample size." The symbol "?" means that such data was not accessible. Abbreviations are as follows: AA, atrium that projects more anteriorly; AEL, anterior extension of liver (i.e., which liver is anteriormost); ALA, anterior liver asymmetry; GbKG, gall bladder–kidney gap; GBM, gall bladder midpoint; GGG, gall bladder–gonad gap; GKG, gonad–kidney gap; GKI, gall bladder–kidney interval; GTL, gonad total length; HLG, heart–liver gap; HLI, heart–liver interval; HMP, heart midpoint; KCG, kidney–cloaca gap; KCI, kidney–cloaca interval; KLI, kidney–liver interval; LA, liver asymmetry; LAdM, left adrenal midpoint; LAL, left atrium length; LGG, liver–gall bladder gap; LGI, liver–gall bladder interval; LKG, liver–kidney gap; LKL, left kidney length; LKM, left kidney midpoint; LLL, left liver length; LLM, left liver midpoint; LTL, left testicle length; LTM, left testicle midpoint; OM, ovaries midpoint; PLA, posterior liver asymmetry; PLRB, posterior limit of right bronchus; RAdM, right adrenal midpoint; RAL, right atrium length; RBL, right bronchus length; RCL, rectal caecum length; RKL, right kidney length; RKM, right kidney midpoint; RLA, right lung anterior limit; RLL, right liver length; RL/LL, right liver/left liver; RLM, right liver midpoint; RLP, right lung posterior limit; RLuL, right lung length; RLuM, right lung midpoint; RTL, right testicle length; RTM, right testicle midpoint; SHI, snout—heart interval; SLT, number of segments in left testicle; SRT, number of segments in right testicle; TAM, total adrenal midpoint; TKL, total kidney length; TKM, total kidney midpoint; TLL, total liver length; TLLS, total number of left liver segments; TLRB, total length of trachea plus right bronchus; TLS, total number of liver segments; TM, testicles midpoint; TMP, trachea midpoint; TRBM, trachea plus right bronchus midpoint; TRLS, total number of right liver segments; TTS, total number of segments in testicles; VL, ventricle length.

juxtaposed in *Tetracheilostoma*, with a gradual distancing between segments posteriorly; while in *Mitophis* the segments are juxtaposed along their length (Figure 20b,c). The right liver is longer than the left (Table 2).

The *gall bladder* (Figure 20d–e) is small, oval, translucid, and located at the pyloric region, always associated with the pancreas and spleen. In *Tetracheilostoma*, a liver-gall bladder gap is absent, while in *Mitophis* it is of 2.9%.

The *pancreas* (Figure 20d) is small and consists exclusively of the ventral lobe, being undivided and located adjacent to the gall bladder. It is subtriangular, creamish yellow and adhered to the duodenum, at the pyloric junction, with its dorsal surface being concave. A *juxtasplenic body* (Figure 20d,e) emerges from the anterior portion of the pancreas, fitting anteromedially to the "complex spleen-gall bladder-pancreas", being light orange. While in *T. bilineata* it is usually smaller than the pancreas, in *M. leptepileptus* it is about three times larger than the latter (Figure 20d,e). The pancreas, spleen and gall bladder are in the anterior part of the posterior half of the body.

The *spleen* (Figure 20e) is rigid, oval, and white, located anteriorly to the pancreas and gall bladder, being smaller than these two organs.

The *testicles* (analyzed exclusively for *M. leptepileptus*, Figure 20f) are multipartite, located in the anterior part of the last third of the body cavity (right testicle at 78.8% and left at 81.2%), being separated from the gall bladder by a short gap (9.5%). They lie slightly anterior to the kidneys, being separated by a gap of 0.8%. The right and left testicles are composed of a total of 9 and 11 segments, respectively.

The *ovaries* (analyzed exclusively in *T. bilineata*) are located between the gall bladder and kidneys, at about the anterior quarter of the body. They are thin and elongate, bearing a right oviduct. A total of five eggs ($n = 1$) are present, being about 4 mm long and of the same width as the body cavity.

The *adrenals* are small (<1%), slightly elongated, light orange in color, and located dorsoposterior to each of the gonads. The right adrenal is slightly anterior to the left, also being longer than the latter (Table 2).

The *kidneys* represent the last paired organs in the body cavity (Table 2) being ellipsoidal, not lobular, and light brown in preserved specimens. Their dorsal surface is convex, while the ventral is concave. The right kidney is longer than the left (Table 2); the left kidney is located more anterior than the right.

The *rectal caecum* represents an evagination of the rectum, being slightly darker than the adjacent intestine. It is reduced (<1%), tubular, not tapering and without any constriction. A *retrocloacal sac* is absent.

4 | DISCUSSION

4.1 | The island rule and the reduced body size of *Mitophis* and *Tetracheilostoma*

The "island rule" represents a phenomenon affecting the size of animals in these isolated environments, with a tendency of large animals to become smaller (= insular dwarfism), and small animals to become larger (= insular gigantism). Even though there has been a long debate whether such evolutionary tendency is in fact applicable to all vertebrates inhabiting islands (see Benton et al., 2010; Meiri, Cooper, & Purvis, 2008; Raia & Meiri, 2006), previous papers indicate that the island rule seems to be best expressed in endothermic animals in comparison to ectothermic ones (e.g., Benton et al., 2010; Clegg & Owens, 2002). Thus, the demonstration of such a trend still needs to be further examined considering large sets of examples from various vertebrate groups (Benton et al., 2010). The "island rule" phenomenon has been previously reported for a few ectothermic groups (Lomolino, 2005), including snakes (e.g., Boback, 2006; Boback & Guyer, 2003; Card et al., 2016; Lomolino, 2005; Reynolds et al., 2016). While examining the assemblages of snakes on islands, Boback and Guyer (2003) reinforced the pattern found in mammals (= island rule), but also found that the extremes of body sizes decrease as the island area decreases. According to the authors, this trend might be associated with energy demands and mechanical constraints on locomotion that impose changes toward an optimal size.

The West Indies represent one of the world′s biodiversity hotspots, with dwarfism being previously registered for vertebrates inhabiting these islands (e.g., Estrada & Hedges, 1996), including snakes (Reynolds et al., 2016). Both *Mitophis* and *Tetracheilostoma* are small snake species that are known to occur exclusively on the islands of Hispaniola and the Lesser Antilles respectively and, according to the biogeographic hypotheses available for the family, the dispersal from an ancestor of leptotyphlopids to these islands might have occurred ~78 Mya through transatlantic dispersal from Africa (Adalsteinsson et al., 2009; Vidal et al., 2010). Such a hypothesis might align with the possibility of the existence of ecological constraints imposed by these islands (e.g., prey availability; soil conditions) upon their colonization, leading to or favoring a reduced body size in these small islands, as previously registered for other taxa therein (Reynolds et al., 2016).

Given the morphological results found in the present study, the reduced size of specimens and considering the tendency toward dwarfism in the West Indies, in the

following section we will discuss the possibility of the phenomenon of miniaturization as the main factor leading to the putative insular dwarfism discussed herein.

4.2 | Miniaturization and its possible relation with the distinct morphology of *Mitophis* and *Tetracheilostoma*

Blindsnakes, threadsnakes, and wormsnakes (traditionally known as "Scolecophidia") are of small size (mostly), fossorial and have extremely modified baupläne, which diverged at the base of the evolutionary radiation of modern snakes (Fachini et al., 2020; Greene, 1997; Vidal et al., 2010). Even though all living lineages, mainly from Anomalepididae and Leptotyphlopidae are small-sized—with an adult maximum size ranging from 106 mm (*Tetracheilostoma carlae*; Adalsteinsson et al., 2009) to 460 mm (*Rhinoleptus koniagui*; Adalsteinsson et al., 2009)—recent fossil discoveries indicate that scolecophidians exhibited large sizes (~1 m) in the Mesozoic and only later underwent an extreme body size reduction (Fachini et al., 2020). Such an extreme evolutionary size reduction—possibly due to miniaturization—most likely occurred independently in each of the main lineages (i.e., Anomalepididae, Leptotyphlopidae, and Typhlopoidea; Fachini et al., 2020).

Miniaturization has independently evolved many times in invertebrates and vertebrates, leading to extremely reduced body-sizes that result in dramatic alterations of morphology, physiology, and ecology of organisms (Hanken, 1983, 1984; Hanken & Wake, 1993). This widespread pattern suggests that selection can often favor its emergence (Glaw et al., 2021; Hanken & Wake, 1993) triggered by the increase in individual fitness via the occupation of new niches, predator avoidance, ingestion of distinct food items, occupation of environments with limited resources, and also promoting rapid reproductive maturity (Hanken & Wake, 1993; Yeh, 2002). Even though miniaturized vertebrates—including living reptiles—have been reported for several lineages, miniaturization is rather much more than achieving a very reduced size. This phenomenon is associated with the occurrence of morphological simplifications, innovations and/or the presence of a high degree of intraspecific variation (Hanken, 1984; Hanken & Wake, 1993). Thus, understanding and recognizing the processes underlying miniaturization remains a complex task and must rely almost exclusively on phenotypic alterations that are described for the taxa.

Morphological consequences of miniaturization (i.e., simplifications and innovations) are often achieved by functional constraints and consequences of heterochrony, manifesting—in vertebrates—as alterations in the skull size or bone presence/absence, extreme ossification of skull elements, fusion of skull elements, and the simplification of limbs such as the loss of phalangeal elements (Yeh, 2002). These heterochronic consequences might be driven by the mechanism of paedomorphism or peramorphism (Hanken, 1993; Rieppel, 1996). While the first phenomenon refers to the retention of ancestrally embryonic or juvenile traits in the adult stage—like reduction or loss of skull elements—peramorphism refers to the expansion of adult development to generate new or even hypertrophied structures (Hanken, 1993).

The "scolecophidian" snakes have long been regarded as miniaturized lineages, although—as far as we are aware—only very few studies have addressed this matter with the discussion of phenotypic consequences driven by this phenomenon (e.g., Chretien, Wang-Claypool, Glaw, & Scherz, 2019; Hedges, 2008; Strong, Palci, & Caldwell, 2021). Recent works (Kley, 2006; Rieppel & Maisano, 2007; Strong et al., 2021) hypothesize that several "typical" scolecophidian characteristics might represent a result of paedomorphosis, such as the lack of medial frontal pillars, of a laterosphenoid, the reduction of palatal and lower jaw elements, and the lack of crests and ridges in the braincase. These authors also reinforce the hypothesis that the autapomorphic conditions found in scolecophidians are indeed related to the specialized miniaturized and fossorial nature of this group. A few additional characters exhibited among scolecophidians, such as their extremely reduced head size (shorter than 15 mm), the presence of a wide parietal fontanelle (e.g., see Broadley & Wallach, 2007; List, 1966) and the loss of an aponeurotic system (Martins, Passos, & Pinto, 2019; Rieppel, 1980) might also represent evidence of miniaturization driven by paedomorphosis, and must be addressed in the future within a phylogenetic context using comparative methods.

Because miniaturization can occur in confluence with fossoriality (Lee, 1998; Rieppel, 1984; Rieppel, 1996; Strong et al., 2021) several traits that will be discussed herein might also be a result of headfirst fossorial habits found in both *Mitophis* and *Tetracheilostoma* (as well as all other known "scolecophidians"). Previous works on squamates that are headfirst burrowers indicate that some characteristics of miniaturization might also be associated with fossoriality (e.g., Hanken & Wake, 1993; Lee, 1998; Rieppel, 1996; Roscito & Rodrigues, 2010), since they generate convergent reinforced skulls with reduced mobility. Previous studies (e.g., Daza, Abdala, Thomas, & Bauer, 2008; Lee, 1998) have also hypothesized that miniaturization might even represent a consequence of headfirst burrowing, considering the reduction of the relationship between the diameter of tunnel and body size might reduce the energy required for

burrowing. Thus, a few structural simplifications of the skull discussed herein, specifically considering those regarding the fusion of posterior skull elements found in both *Mitophis* and *Tetracheilostoma*, and the novelties exhibited by the posteromedial contact of the parietal with the fused prootics + otooccipitals might not be disregarded as a possible effect of their headfirst burrowing habits. A posterior fusion of elements is also convergently found in other fossorial squamates such as amphisbaenians and in a few fossorial nonscolecophidian snakes (Lee, 1998).

Given the extremely reduced size of both *Tetracheilostoma* and *Mitophis* in comparison to other leptotyphlopids (Adalsteinsson et al., 2009; Hedges, 2008), and the three main morphological syndromes driven by miniaturization postulated by Hanken (1984) and Hanken and Wake (1993)—that is, morphological novelties, structural simplification, and high degree of intraspecific variability—we believe that a few osteological and visceral characters are putatively a direct result of the extreme miniaturization in both genera possibly imposed by fossoriality and paedomorphosis that might reflect the "island rule." Each of these morphological consequences will be discussed in the following topics.

4.2.1 | Morphological novelties

Development of morphological novelties seems to functionally compensate for the loss or reduction of elements of vital function in extremely size-reduced lineages (Hanken, 1993). As detailed in the next subsection, most of the variation found in the skull and postcranial skeleton of *Mitophis* and *Tetracheilostoma* seems to be a result of structural simplification. On the other hand, miniaturization in both taxa might have led to morphological novelties mostly in their viscera, possibly attained by the gain of organ segments in parallel to reduction in body length and width.

The snout complex of leptotyphlopids is telescoped (sensu Haas, 1930), with partial overlap among its components, and this configuration might reflect a direct result of strict fossoriality (Bellairs & Kamal, 1981). The organization of the snout complex elements in fossorial snakes also directly reflects on distinct load-bearing forces during excavation (Cundall & Rossman, 1993). The typical "central-rod" and "outer shell" designs proposed by Cundall and Rossman (1993) have been proposed for scolecophidians, although recent papers (e.g., Pinto, Martins, Curcio, & Ramos, 2015; Rieppel et al., 2009) have reinforced that the snout complex of leptotyphlopids incorporates aspects of both designs. This seems to be true for *Mitophis* and *Tetracheilostoma*, with *M. leptepileptus*

exhibiting a distinct configuration of snout elements in comparison with other leptotyphlopids. In leptotyphlopids, the dorsal lamina of the septomaxilla inflects medially to contact the nasal septum dorsally (Koch et al., 2021; Martins et al., 2021; Pinto et al., 2015; Rieppel et al., 2009). In *M. leptepileptus*, besides the medial contact with the nasal septum, the septomaxilla projects dorsally into a laterally compressed flange that contacts the frontals dorsally. As far as we are concerned, this midlateral flange is exclusive to this genus in comparison to all Epictinae. This morphological novelty possibly incorporates aspects of a central-rod design, with the medial bones (mostly the septomaxilla to the frontals posteriorly) representing the main load-bearing elements responsible for dissipating force posteriorly along the midline. Considering the extremely reduced skull of *M. leptepileptus*, we consider that both extreme reduction of size (miniaturization) and the fossorial habits of the species are associated with this morphological novelty. This phenomena might have also led to the distinct configuration of the medial contact with the parietal and the fused prootics + otooccipitals, with the parietal abutting to the anteromedial lamina of these fused elements, in a distinct configuration in comparison with other Epictinae.

The lower jaw of leptotyphlopids is very conserved in comparison to their skull morphology, with most of the variability being reported for total number of teeth and a few variations regarding element shapes—which still do not vary notably—and foramina (Koch, Martins, & Schweiger, 2019; List, 1966; Martins et al., 2019; Pinto et al., 2015; Rieppel et al., 2009; Salazar-Valenzuela, Martins, Amador-Oyola, & Torres-Carvajal, 2015). Both the suspensorium and mandible of *Tetracheilostoma* are remarkably similar and are in accordance with the conservative nature of this morphofunctional unit, resembling other Epictinae genera. However, the lower jaw of *Mitophis* exhibits a few modifications that somehow set aside the conservative nature of the lower jaw in leptotyphlopids. In this taxon, the quadrate exhibits a distinct and stout posterior process that is unique among the Epictinae. A posterior elongation of the quadrate (= suprastapedial process) is present in several basal snakes such as *Cylindrophis* and *Uropeltis* (Cundall & Irish, 2008; Garberoglio et al., 2019; Rieppel, 1980) and fossil taxa such as *Dinilysia* and *Najash* (Garberoglio et al., 2019). However, it is unclear if the posterior process found in *Mitophis* is homologous to the suprastapedial process of alethinophidian snakes. Nonetheless, as in alethinophidians (see Rieppel, 1980), the *Musculus depressor mandibulae* of *Mitophis* originates on the ventral lamina of the posterior process of the quadrate (= suprastapedial process of alethinophidians; Martins et al., 2019) and inserts onto the mandible more

anteriorly, indicating that these regions might be homologous. However, additional sources of data must be addressed in the future to clarify the nature of the posterior process of the quadrate found in *Mitophis*, especially when attempting to establish this character as either plesiomorphic, or as a morphological novelty attained by the necessity of head morphology rearrangement as a consequence of miniaturization. If considering the second condition, this extremely developed posterior element might have been gained through peramorphosis, by the extreme ossification of its proximal epiphysis (see Pinto et al., 2015).

Regarding the trunk, cloacal, and caudal vertebrae, our results show that they are very similar to other leptotyphlopids in terms of their morphology (as mentioned above)—except for the caudal morphology of *Mitophis* (as will be further discussed). The total number of trunk vertebrae of Epictinae varies from 152 to 391 (Koch et al., 2019; Martins, 2016; Martins, Koch, et al., 2019; Pinto et al., 2015), with *Tetracheilostoma* representing the minimum and *Mitophis* representing the maximum of this range within the subfamily. *Mitophis* also represents the maximum of the interval of 2–6 cloacal vertebrae within the family (Martins, 2016; Martins et al., 2021; Martins, Koch, et al., 2019; Pinto et al., 2015). Such extremes in number of vertebrae might suggest that both lineages have dealt with miniaturization by diverging in two opposite pathways: augmenting the number of vertebrae to possibly compensate for the extremely reduced body circumference in the case of *Mitophis*, and the reduction of total vertebrae to obtain a shorter and miniaturized body in *Tetracheilostoma*. In this sense, vertebrae number in *Mitophis* might be regarded as a morphological novelty, whereas *Tetracheilostoma*—when considering the mean vertebrae number in Epictinae—represents a structural simplification. The mechanism of generation of such an apomorphic character needs to be further investigated in terms of its evolutionary development scenario.

Regarding visceral data, while *Tetracheilostoma* seems to be similar to other leptotyphlopids in terms of its gross morphology, *M. leptepileptus* distinguishes from the majority of leptotyphlopids based on the variation in terms of total number of liver and of testicle segments. Leptotyphlopids usually exhibit a mean of ~37 liver segments (right lobe; Martins, 2016; Wallach, 1998a, 1998b), while in *M. leptepileptus* we observed a total of 54 segments, representing a much higher number in comparison to all Epictinae (Martins, 2016; Wallach, 1998a, 1998b). The same is true for the total number of testicle segments: previous data for Epictinae report a total of 2–6 segments in each testicle, but the number found for *M. leptepileptus* was much higher, with 9 and 11 segments in the right and left testicle, respectively. As postulated

by Hanken (1984) and Hanken and Wake (1993) the extreme reduction of body size achieved by miniaturization might involve novel features in an individual to compensate for physiological demands constrained by body size reduction. Therefore, the extremely reduced body circumference found in *Mitophis* might have been compensated by the gain of additional organ segments—or even the opposite, with the gain of segments allowing the extreme body miniaturization. Such a gain would putatively compensate the organ reduction by enlarging the surface area of the organ with additional segments, therefore relaxing the physiological constraints imposed by the extremely reduced body width.

Most miniaturized tetrapods exhibit a relatively reduced number of offspring possibly triggered by the constraints imposed by their limited body cavity (Estrada & Hedges, 1996; Hedges, 2008; Rensch, 1948). Hedges (2008) reports such a constraint in *T. carlae*, with the presence of a single elongated egg, and discusses the constraints in egg shape and size related to offspring size. We were able to observe the presence of five eggs in a single female specimen of *T. bilineata*. All five eggs were elongated, with 4 mm length, differing from *T. carlae* and from the typical interval of 1–3 eggs in small species of snakes (Fitch, 1970; Hedges, 2008). Even though the relatively high number of eggs in *T. bilineata* seems impressive, it follows the relationship of egg size, clutch size and body shape in snakes, where a higher number of eggs results in shorter egg length/width ratio (Hedges, 2008), as it was found herein for *T. bilineata*. Therefore, clutch size seems to greatly vary in *Tetracheilostoma* and must be further evaluated from an evolutionary perspective considering putative output differences found between *T. carlae* and *T. bilineata*.

4.2.2 | Structural simplification

The reduction of body size within a lineage is accompanied by modifications and changes of structural proportions in their morphology, physiology, ecology, and behavior (Hanken & Wake, 1993). Such a reduction might be attained by reducing tissue cell layers, therefore minimizing their size and volume (Rensch, 1948). Consequently, some body structures (such as organs, tissues, etc.) might be completely lost, and the remaining structures need to be reorganized to compensate for their loss or reduction (Hanken, 1993; Rensch, 1948). Structural simplifications have been the best-documented consequences of miniaturization among tetrapods (e.g., Daza et al., 2008; Hanken, 1984; Rieppel, 1996). The reduction or loss of both skull and lower jaw elements in *Mitophis* and *Tetracheilostoma* might have led to the

rearrangement of their related morphological components, for instance, their difference in the muscular arrangement in comparison to other Epictinae (Martins et al., 2018; Martins, Koch, et al., 2019; present study), such as their extremely reduced *Musculus levator anguli oris* (Martins, Koch, et al., 2019). The rearrangement of head muscles in miniaturized lineages in response to extremely miniaturized skulls has also been previously reported in the literature for other squamates (e.g., Daza et al., 2008).

The fusion of a few dorsal elements of the braincase, and the extreme simplification of the maxilla found in both *Mitophis* and *Tetracheilostoma* are unique among Epictinae (i.e., Koch et al., 2019; List, 1966; Martins, Koch, et al., 2019; Pinto et al., 2015; Rieppel et al., 2009; Salazar-Valenzuela et al., 2015). In all members of this subfamily (except for *Mitophis* and *Tetracheilostoma*), the maxilla is a wide and laterally compressed element that covers most of the ascending process of the septomaxilla in lateral view, also providing a lateral limit for the nasal gland (Koch et al., 2019; List, 1966; Martins et al., 2018; Martins, Koch, et al., 2019; Pinto et al., 2015; Rieppel et al., 2009; Salazar-Valenzuela et al., 2015). This element also bears a rectangular and perforated ventral lamina known as the dentigerous process. In both *Mitophis* and *Tetracheilostoma*, a dentigerous process is absent, and the anterior process that provides a dorsal cover for the nasal gland is reduced (present study). In *Mitophis*, the maxillae are extremely reduced (i.e., simplified), laminar, and do not participate in any level of the lateral cover of the snout, representing a very distinctive feature among Epictinae lineages. Additionally, *Tetracheilostoma* spp. also differ from other Epictinae in having the maxillary process—which usually contacts or almost contacts the posterior lamina of the prefrontal—abutting posteriorly to the septomaxilla. As evident from previous studies on snake development (e.g., Boughner et al., 2007; Mohammadi, Khannoon, & Evans, 2019; Polachowski & Werneburg, 2013; Vonk et al., 2008), the simplification of the maxillae in *Mitophis* and *Tetracheilostoma* might reflect a result of paedomorphism, since earlier embryonic stages reflect the simple and poorly-developed conditions of these elements. However, these studies are based on alethinophidian snake taxa, and future studies on the development of leptotyphlopids are needed. Finally, the condition found in the palatomaxillary elements of *Mitophis* and *Tetracheilostoma* likely represents an unequivocal synapomorphy for the subtribe Tetracheilostomina, also being taxonomically relevant for the distinction of taxa at a generic level.

The dorsoposterior elements of the skull in Epictinae are usually composed of the supraoccipitals (less commonly fused into a single plate in a few taxa; see Martins et al., 2021), prootics and otooccipitals, the latter forming most of the dorsal and lateral margins of the foramen magnum (Koch et al., 2019; List, 1966; Martins, Koch, et al., 2019; Pinto et al., 2015; Rieppel et al., 2009; Salazar-Valenzuela et al., 2015). In *Mitophis* and *Tetracheilostoma*, however, these dorsoposterior elements underwent major modifications in relation to their New World congeners, as follows. *M. leptepileptus* exhibits a dorsoposterior pentagonal element, which we herein refer to as the supraoccipital based on topology and muscle insertion (see Martins, Passos, & Pinto, 2019). Although its homology needs further evidence, this element is medially located to the structure considered as the fused prootic + otooccipital, in such an organization that resembles the condition found in a few Anomalepididae taxa such as: *Helminthophis praeocularis* (Curcio, 2003) and *Liotyphlops albirostris* (List, 1966; Rieppel et al., 2009). However, the posterior extension of this element to exclude the otooccipitals in the formation of the dorsal cover of the foramen magnum is unique among all Leptotyphlopidae and also when considering the currently recognized "Scolecophidia" (Haas, 1964, 1968; List, 1966; Rieppel et al., 2009). Thus, it represents an apomorphic character state for the genus that might be triggered by extreme miniaturization, even though the developmental causes still need to be unraveled. The genus *Tetracheilostoma*, on the other hand, does not exhibit any trace of a distinct supraoccipital. We hypothesize that the supraoccipital is fused to the parietal in *Tetracheilostoma* given that in all Epictinae the parietal ends in an approximately slightly convex suture, contacting the prootics, and supraoccipitals (Koch et al., 2019, 2021; List, 1966; Martins et al., 2021; Martins, Koch, et al., 2019; Pinto et al., 2015; Rieppel et al., 2009). As the fusion of skull elements is very common in miniaturized species (Yeh, 2002), we suggest herein that the possible fusion of the parietal with the supraoccipitals into a wide plate may be due to miniaturization effects, although one may not disregard the association of such a fusion as a direct result of fossoriality. Such an assumption is also likely for the fusion of the prootic + otooccipital that occurs in both genera (present study), but does not occur in any other Epictinae so far described (e.g., Koch et al., 2019; List, 1966; Martins, Koch, et al., 2019; Pinto et al., 2015; Rieppel et al., 2009; Salazar-Valenzuela et al., 2015).

The precloacal, cloacal, and caudal vertebrae are very conserved among "scolecophidians" (Fachini et al., 2020; Holman, 2000; List, 1966) in such a way that they are all dorsoventrally flattened, bear synapophyses with a single articular facet, lack a neural spine, and exhibit a rounded cotyle and condyle (Holman, 2000; Koch et al., 2019; List, 1966; Martins, Koch, et al., 2019; Pinto et al., 2015).

The cervical vertebrae (i.e., atlas and axis) usually vary in terms of the presence/absence and shape of the intercentrum I, and in the shape of the intercentra II and III for the axis, with the former usually being very conserved intergenerically among Epictinae (Koch et al., 2019; Martins, Koch, et al., 2019; Pinto et al., 2015). In *Mitophis* and *Tetracheilostoma*, an intercentrum I is absent (present study), contrasting with the well-developed intercentrum I of *Trilepida* and *Rena* (Martins, 2016; Pinto et al., 2015). A few *Epictia* spp. might also exhibit a reduced or absent intercentrum I (Martins, 2016; Koch et al., 2019, 2021), and thus such a feature is not exclusive to Tetracheilostomina. As in squamates the neural arch ossifies first, with several other vertebral regions (e.g., synapophyses, zygapophyses, and zygosphenes) chondrifying later in the development as outgrowths of the neural arches (Boughner et al., 2007; Winchester & Bellairs, 1977), the truncation of the intercentrum I development in these snakes might be accomplished by the retention of embryonic stage in adults (i.e., paedomorphosis), reflecting heterochronic implications in vertebral morphology. As detailed below, these heterochronic phenomena might also apply to the caudal vertebrae structure of both lineages.

The caudal vertebrae of all known snakes—including fossil lineages—are known for the absence of ribs, and the presence of lateral conspicuous processes known as pleurapophyses (Holman, 2000). In both specimens analyzed herein of *M. leptepileptus* (μCT and cleared and stained), the pleurapophyses are absent, and instead a short inconspicuous rounded projection is present in their place. Such absences are then a unique condition found within all snakes, and this character must be examined in additional *Mitophis* spp. to evaluate if this loss is shared among their congeners. The absence of pleurapophyses (= transverse processes; Etheridge, 1967) is common in a few lineages of "lizards" (i.e., Iguanidae and Agamidae; Etheridge, 1967), but the extreme reduction in *Tetracheilostoma* and its absence in *M. leptepileptus* might be explained by a morphological simplification driven by a paedomorphic event, with the truncation of the pleurapophyseal development being attained by the retention of embryonic stage in the adults. Therefore, these characteristics are unique and autapomorphic for these taxa.

Rudimentary pelvic elements exhibit variable levels of degeneration among snakes, with such a level of degeneration most likely indicating their feasible functional aspect rather than their vestigial retention (Palci et al., 2020). Leptotyphlopids in general exhibit a low degree of degeneration of pelvic and hindlimb elements among snakes (Essex, 1927; List, 1966; Palci et al., 2020), with the presence of four ossified (and rarely cartilaginous)

distinctive elements (ilium, ischium, pubis, and femur; Pinto et al., 2015; Palci, Hutchinon, Caldwell, Smith, & Lee, 2019; Martins et al., 2021). Both *Mitophis* (except for *M. calypso*) and *Tetracheilostoma*, however, seem to lack any trace of an ossified rudimentary pelvic element. However, most of our examinations were based on radiographies and we do not disregard the fact that these elements might be present with a low degree of ossification or even being totally cartilaginous in the specimens analyzed through radiographies. Even though there seems to be a small cartilaginous rod-like structure in the cleared and stained specimen of *M. leptepileptus*, we are not sure whether it might consist of any vestige of a pelvic element, or if it is purely a bias from the clearing and staining process. In any case, the complete (or almost complete) absence of any rudimentary pelvic element in these taxa (also confirmed in X-rayed specimens) would align with the hypothesis of their reversion considering the potential that the snake ancestral lineage lacked pelvic elements (Palci et al., 2019). If all *Mitophis*—except for *M. calypso*—indeed lack rudimentary pelvic elements, the presence of these structures in the latter must be further evaluated from an evolutionary perspective. Finally, as limbs develop in early stages of the embryonic development, but after the total development of vertebrae (Boughner et al., 2007), the lack of pelvic rudiments or even their presence by the retention of a rod cartilaginous element in *Mitophis* spp. might reflect a paedomorphic retention of early snake embryonic stage.

4.2.3 | Intraspecific variation

Increased intraspecific morphological variation is one of the main consequences of body miniaturization (Hanken, 1993). When present, it can be the result of truncated development or emerge because of the early development of structures (Hanken, 1993). Even though our specimen samples were very limited in this study, mostly because these taxa are poorly represented in museum collections, the variation of the either paired or fused condition of the parietal remains as a noticeable morphological novelty that varied in *M. leptepileptus*. As the parietal bone fuses in later stages of the embryonic development (e.g., Mohammadi et al., 2019), the paired condition found in "scolecophidians" must be regarded as the result of truncated development. The presence of a paired condition of this bone occurs in a few leptotyphlopids, but has also been reported for extremely autapomorphic and miniaturized typhlopoid taxa (Chretien et al., 2019). The high degree of intraspecific variation due to truncated development has also been reported for several other miniaturized vertebrate taxa

(e.g., Hanken, 1993; Yeh, 2002). Therefore, the intraspecific variation found in the condition of the parietal in *M. leptepileptus* is most likely a result of morphological novelty driven by miniaturization.

The general aspect of the mandible of *Mitophis* and *Tetracheilostoma* and their elements' morphology is rather similar to other Epictinae in being long and with a specialized intramandibular joint, except for a noticeable dorsoventrally flattened aspect that contrasts with the dorsally wide aspect exhibited by other Epictinae (Koch et al., 2019; List, 1966; Martins, Koch, et al., 2019; Pinto et al., 2015; Rieppel et al., 2009; Salazar-Valenzuela et al., 2015). However, in *Mitophis* the splenial varies in shape, with one specimen being distinct from other Epictinae in not being elongate—it is rather a short and triangular element that expands dorsally, consequently widening the cotyle-condyle area for the movable intramandibular joint. This dorsal expansion (= morphological novelty) might have arisen from the conflicting pressures of size reduction associated with the need for maintenance of the regular function for the intramandibular joint to allow for underground feeding. However, their underlying developmental causes are yet to be unravelled.

4.3 | Morphology and the systematic implications for genera diagnosis

Leptotyphlopids, as well as several other "scolecophidians" exhibit a very conserved external morphology, which summed to a few other factors (e.g., limited specimen samples in collections) have led to an obscurity in their taxonomy in the past decades. Even though the first studies regarding the leptotyphlopid internal morphology are dated back from the 19th century (e.g., Duméril & Bibron, 1844), the first mention to the utility of osteological data for the diagnosis of genera and even species within leptotyphlopids only arose a few decades ago (Broadley & Broadley, 1999). The past few years have witnessed the increase of contributions on the osteology of leptotyphlopids (e.g., Koch et al., 2019; Koch et al., 2021; Martins et al., 2021; Martins, Passos, & Pinto, 2019; Salazar-Valenzuela et al., 2015), reinforcing the utility of these data in the systematics of the family. Similarly, studies on snake visceral morphology and topography represent relevant sources of systematic data, being historically applied to the proposition of new supraspecific taxa, as well as employed in species delimitation (e.g., Underwood, 1967; Wallach and Ineich, 1996; Wallach and Gunther, 1997; Wallach and Smith, 1992). The topography of viscera is extremely relevant in terms of its significance since visceral variation represents direct results of body elongation added to their

obvious functional constraints. Even though the morphology and topography of viscera are feasible for distinguishing the major taxa among "Scolecophidia" (i.e., Anomalepididae, Leptotyphlopidae, and Typhlopoidea), these data are relatively conserved at some taxonomic rank such as interspecifically or intergenerically (Wallach, 1998a, 1998b; Martins, 2016).

All morphological characters gathered herein allow us to distinguish both *Mitophis* and *Tetracheilostoma* from all other Epictinae by a combination of characters, as follows. The genus *Mitophis* distinguishes from all other Epictinae by exhibiting a single pentagonal supraoccipital bone that participates in the formation of the foramen magnum (vs. fused or paired, but not participating in the foramen magnum), by the total or conspicuous degeneration of the pelvic elements (vs. not conspicuously degenerated and composed of an ilium, ischium, femur, and pubis), and by the high number (=54) of liver segments (vs. ~30); from all Epictinae, except for *Tetracheilostoma* by the fusion of the prootic to the otooccipital into a single plate (vs. distinct elements), and by the absence of a maxillary dentigerous process; from *Rena* by its paired nasal bones (vs. fused); from *Trilepida* and *Rena* by the otooccipitals excluding the basioccipital from the formation of the foramen magnum and by the absence of an intercentrum I (vs. present and well-developed). The genus *Tetracheilostoma* differs from all other Epictinae by the absence of a supraoccipital bone, which is most likely fused to the parietal bone; from all other Epictinae except for *Mitophis* by the fused prootic + otooccipital (vs. distinct elements) and the lack of a maxillary dentigerous process; from *Rena* by the paired nasals (vs. fused); from *Trilepida* and *Rena* by the otooccipitals excluding the basioccipital from the formation of the foramen magnum (vs. participating) and the absence of an intercentrum I (vs. present and well-developed).

5 | CONCLUSION

Herein, we hypothesize that most novelties and simplifications of the viscera and osteology observed in both *Mitophis* and *Tetracheilostoma* are a direct result of their extreme miniaturization. Even though scolecophidians are known for their miniaturized morphology most likely driven by paedomorphosis, our study brings novel data on the extreme miniaturization of both genera, most of which may also be driven by paedomorphosis and/or fossoriality. These data must be further evaluated from an evolutionary perspective, mainly regarding the "island rule" and using comprehensive phylogenetic hypotheses. Since these are not

the only miniaturized tetrapods from the West Indies, these islands possibly represent great places for the evaluation of macroevolutionary patterns toward dwarfism. The examination of scolecophidian skeletal ontogeny will be a fundamental breakthrough to identify the heterochronic processes underlying their autapomorphies.

AUTHOR CONTRIBUTIONS

Claudia Koch: Formal analysis; investigation; methodology; software; writing-review & editing. **Mitali Joshi:** Software; writing-review & editing. **Alessandra Machado:** Formal analysis; investigation; methodology; software; visualization; writing-review & editing. **Ricardo Lopes:** Funding acquisition; methodology; software; writing - original draft. **Paulo Passos:** Conceptualization; funding acquisition; project administration; writing - original draft; writing-review & editing.

ORCID

Angele Martins https://orcid.org/0000-0002-0193-4011
Claudia Koch https://orcid.org/0000-0002-7115-2816

REFERENCES

Adalsteinsson, S. A., Branch, W. R., Trape, S., Vitt, L. J., & Hedges, S. B. (2009). Molecular phylogeny, classification, and biogeography of snakes of the family Leptotyphlopidae (Reptilia, Squamata). *Zootaxa, 2244*, 1–50.

Bellairs, A. A., & Kamal, A. M. (1981). The chondrocranium and the development of the skull in recent reptiles. In C. Gans & T. S. Parsons (Eds.), *Biology of reptilia* (Vol. 11, pp. 1–263). London: Academic Press.

Benton, M. J., Csiki, Z., Grigorescu, D., Redelstorff, R., Sander, P. M., Stein, K., & Weishampel, D. B. (2010). Dinosaurs and the Island rule: The dwarfed dinosaurs from Hateg Island. *Palaeogeography, Palaeoclimatology, Palaeoecology, 293*, 438–454.

Boback, S. M. (2006). A morphometric comparison of Island and mainland boas (*boa constrictor*) in Belize. *Copeia, 2006*, 261–267.

Boback, S. M., & Guyer, C. (2003). Empirical evidence for an optimal body size in snakes. *Evolution, 57*, 345–351.

Boughner, J. C., Buchtová, M., Fu, K., Diewert, V., Hallgrímsson, B., & Richman, J. M. (2007). Embryonic development of *Python sebae* – I: Staging criteria and macroscopic skeletal morphogenesis of the head and limbs. *Zoology, 110*, 212–230.

Boulenger, G. A. (1893). *Catalogue of snakes in the British museum (natural history)* (Vol. 1). London: Trustes of the British Museum.

Broadley, D. G., & Broadley, S. (1999). A review of the African worm snakes from south of latitude 12°S (Serpentes: Leptotyphlopidae). *Syntarsus, 5*, 1–36.

Broadley, D. G., & Wallach, V. (2007). A revision of the genus *Leptotyphlops* in northeastern Africa and southwestern Arabia (Serpentes: Leptotyphlopidae). *Zootaxa, 1408*, 1–78.

Card, D. C., Adams, R. H., Schield, D. R., Perry, B. W., Corbin, A. B., Pasquesi, G. I. M., … Castoe, T. A. (2016). Genomic basis of convergent Island phenotypes in *boa constrictor*. *Genome Biology and Evolution, 11*, 3123–3143.

Chretien, J., Wang-Claypool, C. Y., Glaw, F., & Scherz, M. D. (2019). The bizarre skull of *Xenotyphlops* sheds lights on synapomorphies of Typhlopoidea. *Journal of Anatomy, 234*, 637–655.

Clegg, S. M., & Owens, P. F. (2002). The 'Island rule' in birds: Medium body size and its ecological explanation. *Proceedings of the Royal Society of London B, 269*, 1359–1365.

Cundall, D., & Irish, F. (2008). The snake skull. In H. Morphology, C. Gans, A. S. Gaunt, & K. Adler (Eds.), *Biology of the reptilia* (Vol. 20, pp. 349–692). New York, NY: Society for the Study of Amphibians and Reptiles.

Cundall, D., & Rossman, D. (1993). Cephalic anatomy of the rare Indonesian snake Anomochilus weberi. *Zoological Journal of the Linnean Society, 109*, 235–273.

Curcio, F. Osteologia craniana comparada e filogenia da Família Anomalepidiidae Taylor, 1939 (Serpentes, Scolecophidia). Unpublished Thesis. 2003.

Daza, J. D., Abdala, V., Thomas, R., & Bauer, A. M. (2008). Skull anatomy of the miniaturized gecko *Sphaerodactylus roosevelti* (Squamata: Gekkota). *Journal of Morphology, 269*, 1340–1364.

Duméril, A. M. C. & Bibron, G.. (1844). Erpétologie générale ou histoire naturelle complète des reptiles. Tome sixième, contenant l'histoire générale des ophidiens, la description des genres et des espèces de serpents non venimeux, savoir: la totalité desvermiformes ou des scolécophides, et partie des cicuriformes ou azémiophides), en tout vingt–cinq genres et soixante–cinq espèces. Paris: Librairie Encyclopédique de Roret.

Esquerré, D., Donnellan, S., Brennan, I. G., Lemmon, A. R., Lemmon, E. M., Zaher, H., … Keogh, J. S. (2020). Phylogenomics, biogeography, and morphometrics reveal rapid phenotypic evolution in pythons after crossing Wallace's line. *Systematic Biology, 69*, 1039–1051.

Essex, R. (1927). Studies in reptilian degeneration. *Proceedings. Zoological Society of London, 4*, 879–945.

Estrada, A. R., & Hedges, S. B. (1996). At the lower size limit in tetrapods: A new diminutive frog from Cuba (Leptodacrtylidae: *Eleutherodactylus*). *Copeia, 1996*, 852–859.

Etheridge, R. (1967). Lizard Caudal Vertebrae. *Copeia, 1967*, 699–721.

Fachini, T. S., Onary, S., Palci, A., Lee, M. S. Y., Bronzati, M., & Hsiou, A. S. (2020). Cretaceous Blind Snake from Brazil Fills Major Gap in Snake Evolution. *iScience*, *23*, (12), 101834. https://doi.org/10.1016/j.isci.2020.101834.

Fitch, H. S. (1970). *Reproductive cycles in lizards and snakes*. Kansas: The University of Kansas Museum of Natural History.

Foster, J. B. (1964). Evolution of mammals on islands. *Nature*, *202*, 234–235.

Garberoglio, F. F., Apesteguía, S., Simões, T. R., Palci, A., Gómez, R. O., Nydam, R. L., ... Caldwell, M. W. (2019). New skulls and skeletons of the cretaceous legged snake *Najash*, and the evolution of the modern snake body plan. *Science Advances*, *11*, 1–8.

Glaw, F., Köhler, J., Hawlitschek, O., Ratsoavina, F. M., Rakotoarison, A., Scherz, M. D., & Vences, M. (2021). Extreme miniaturization of a new amniote vertebrate and insights into the evolution of genital size in chameleons. *Scientific Reports*, *2522*, 11–15.

Gould, S. J. (2002). *The structure of evolutionary theory*. New York, NY: Harvard University Press.

Grant, P. R. (1998). *Evolution on islands*. New York, NY: Oxford University Press.

Greene, H. W. (1997). *Snakes: The evolution of mystery in nature*. Berkeley: University of California Press.

Haas, G. (1930). Ueber das kopfskelett und die kaumuskulatur der typhlopiden und glauconiiden. *Zoologische Jahrbücher. Abteilung für Anatomie Und Ontogenie der Tiere*, *52*, 1–94.

Haas, G. (1964). Anatomical observations on the head of Liotyphlops albirostris (Typhlopidae, Ophidia). *Acta Zoologica*, *45*, 1–62.

Haas, G. (1968). Anatomical observations on the head of Anomalepis aspinosus (Typhlopidae, Ophidia). *Acta Zoologica*, *49*, 62–139.

Hanken, J. (1983). Miniaturization and its effects on cranial morphology in plethodontid salamanders, genus *Thorius* (Amphibia, Plethodontidae): II. The fate of the brain and sense organs and their role in skull morphogenesis and evolution. *Journal of Morphology*, *177*, 255–268.

Hanken, J. (1984). Miniaturization and its effects on cranial morphology in plethodontid salamanders, genus *Thorius* (Amphibia: Plethodontidae). I. Osteological variation. *Biological Journal of the Linnean Society*, *23*, 55–75.

Hanken, J. (1993). Adaptation of bone growth to miniaturization of body size. In B. K. Hall (Ed.), *Bone Growth – B* (Vol. 7, pp. 79–104). Boca Raton, FL: CRC Press.

Hanken, J., & Wake, D. B. (1993). Miniaturization of body size: Organismal consequences and evolutionary significance. *Annual Review of Ecology, Evolution, and Systematics*, *24*, 501–519.

Hedges, S. B. (2008). At the lower size limit in snakes: Two new species of threadsnakes (Squamata: Leptotyphlopidae: *Leptotyphlops*) from the Lesser Antilles. *Zootaxa*, *1841*, 1–30.

Holman, J. A. (2000). *Fossil snakes of North America: Origin, evolution, distribution, paleoecology*. Indiana: Indiana University Press.

Keogh, J. S., Scott, I. A. W., & Hayes, C. (2005). Rapid and repeated origin of insular gigantism and dwarfism in Australian Tiger snakes. *Evolution*, *59*, 226–236.

Kley, N. J. (2006). Morphology of the lower jaw and suspensorium in the Texas blindsnake, *Leptotyphlops dulcis* (Scolecophidia: Leptotyphlopidae). *Journal of Morphology*, *267*, 494–515.

Koch, C., Martins, A. R., Joshi, M., Pinto, R. R., & Passos, P. (2021). Osteology of the enigmatic threadsnake species *Epictia unicolor* and *Trilepida guayaquilensis* (Serpentes, Leptotyphlopidae) with generic insights. *The Anatomical Record*. https://doi.org/10.1002/ar.24676.

Koch, C., Martins, A. R., & Schweiger, S. (2019). A century of waiting: Description of a new *Epictia* gray, 1845 (Serpentes: Leptotyphlopidae) based on specimens housed for more than 100 in the collection of the Natural History Museum Vienna (NMW). *PeerJ*, *7*, e7411. https://doi.org/10.7717/peerj.7411

Lee, M. S. Y. (1998). Convergent evolution and character correlation in burrowing reptiles: Towards a resolution of squamate relationships. *Biological Journal of the Linnean Society*, *65*, 369–453.

Lillywhite, H., & Martins, M. (2019). *Islands and snakes: Isolation and adaptive evolution*. New York, NY: Oxford University Press.

List, J. C. (1966). Comparative osteology of the snake families Typhlopidae and Leptotyphlopidae. *Illinois Biological Monographs*, *36*, 1–112.

Lomolino, M. V. (1985). Body size of mammals on islands: The Island rule re-examined. *The American Naturalist*, *125*, 310–316.

Lomolino, M. V. (2005). Body size evolution in insular vertebrates: Generality of the Island rule. *Journal of Biogeography*, *32*, 1683–1699.

Losos, J. B. (2011). *Lizards in a evolutionary tree: Ecology and adaptive radiation of anoles*. Los Angeles, CA: University of California Press.

MacArthur, R. H. & Wilson, E. O. (2001). *The theory of Island biogeography*. Princeton, NJ: Princeton University Press. New York, NY: Oxford University Press.

Martins, A. R. (2016). *Morfologia Interna Comparada de Representantes da Subfamília Epictinae (Serpentes, Scolecophidia, Leptotyphlopidae)*. (Unpublished Thesis). Rio de Janeiro.

Martins, A. R., Koch, C., Joshi, M., Pinto, R. R., & Passos, P. (2021). Picking up the threads: Comparative osteology and associated cartilaginous elements for members of the genus *Trilepida* Hedges, 2011 (Serpentes, Leptotyphlopidae) with new insights on the Epictinae systematics. *The Anatomical Record*, In press.

Martins, A. R., Koch, C., Pinto, R. R., Folly, M., Fouquet, A., & Passos, P. (2019). From the inside out: Discovery of a new genus of threadsnakes based on anatomical and molecular data, with discussion of the leptotyphlopid hemipenial morphology. *Journal of Zoological Systematics and Evolutionary Research*, *57*, 840–863.

Martins, A. R., Passos, P., & Pinto, R. R. (2018). Unveiling diversity under the skin: Comparative morphology study of the cephalic glands in threadsnakes (Serpentes: Leptotyphlopidae: Epictinae). *Zoomorphology*, *137*, 433–443.

Martins, A. R., Passos, P., & Pinto, R. R. (2019). Moving beyond the surface: Comparative head and neck myology of threadsnakes (Epictinae, Leptotyphlopidae, Serpentes), with comments on the 'scolecophidian' muscular system. *PLoS One*, *14*, e0219661.

Martins, M., & Lillywhite, H. B. (2019). Ecology of snakes on islands. In H. B. Lillywhite & M. Martins (Eds.), *Islands and snakes: Isolation and adaptive evolution* (pp. 1–44). USA: Oxford University Press.

Meiri, S., Cooper, N., & Purvis, A. (2008). The Island rule: Made to be broken? *Proceedings of the Royal Society B*, 275, 141–148.

Millien, V. (2006). Morphological evolution is accelerated among Island mammals. *PLoS Biology*, 4, 1863–1868.

Mohammadi, A. G. A. A. L., Khannoon, E. R., & Evans, S. E. (2019). The development of the osteocranium in the snake *Psammophis sibilans* (Serpentes: Lamprophiidae). *Journal of Anatomy*, 236, 117–131.

Palci, A., Hutchinon, M., Caldwell, M., Smith, K., & Lee, M. (2019). The homologies and evolutionary reduction of the pelvis and hindlimbs in snakes, with the first report of ossified pelvic vestiges in an anomalepidid (*Liotyphlops beui*). *Zoological Journal of the Linnean Society*, 188, 1–23.

Palci, A., Hutchinson, M. N., Caldwell, M. W., Smith, K. T., & Lee, M. S. Y. (2019). The homologies and evolutionary reduction of the pelvis and hindlimbs in snakes, with the first report of ossified pelvic vestiges in an anomalepidid (Liotyphlops beui). *Zoological Journal of the Linnean Society*. https://doi.org/10.1093/zoolinnean/zlz098.

Pinto, R. R., Martins, A. R., Curcio, F. F., & Ramos, L. O. (2015). Osteology and cartilaginous elements of *Trilepida salgueiroi* Amaral, 1954 (Scolecophidia: Leptotyphlopidae). *The Anatomical Record*, 298, 1722–1747.

Polachowski, K. M., & Werneburg, I. (2013). Late embryos and bony skull development in Bothropoides jararaca (Serpentes, Viperidae). *Zoology*, 116, 36–63.

Raia, P., & Meiri, S. (2006). The Island rule in large mammals: Paleontology meets ecology. *Evolution*, 60, 1731–1742.

Rensch, B. (1948). Histological changes correlated with evolutionary changes of body size. *Evolution*, 2, 218–230.

Reynolds, R. G., Collar, D. C., Pasachnik, S. A., Niemiller, M. L., Puente-Rolón, A. R., & Revell, L. J. (2016). Ecological specialization and morphological diversification in greater Antillean boas. *Evolution*, 70, 1882–1895.

Rieppel, O. (1980). The trigeminal jaw adductors of primitive snakes and their homologies with the lacertilian jaw adductors. *Journal of Zoology*, 190, 447–471.

Rieppel, O. (1996). Miniaturization in tetrapods: Consequences for skull morphology. In P. J. Miller (Ed.), *Miniature vertebrates: The implications of small body size (Zoological Symposium no. 69)* (pp. 15–45). Oxford: Clarendon Press.

Rieppel, O., Kley, N. J., & Maisano, J. A. (2009). Morphology of the skull of the white-nosed blindsnake, *Liotyphlops albirostris* (Scolecophidia: Anomalepididae). *Journal of Morphology*, 270, 536–557.

Rieppel, O., & Maisano, J. A. (2007). The skull of the rare Malaysian snake *Anomochilus leonardi* Smith, based on high-resolution X-ray computed tomography. *Zoological Journal of the Linnean Society*, 149, 671–685.

Rieppel, O. (1984). Miniaturization of the lizard skull: its functional and evolutionary implications. *Symposia of the Zoological Society of London*, 52, 503–520.

Roscito, J. G., & Rodrigues, M. T. (2010). Comparative cranial osteology of fossorial lizards from the tribe Gymnophthalmini (Squamata, Gymnophthalmidae). *Journal of Morphology*, 271, 1352–1365.

Salazar-Valenzuela, D., Martins, A. R., Amador-Oyola, L., & Torres-Carvajal, O. (2015). A new species and country record of threadsnakes (Serpentes: Leptotyphlopidae: Epictinae) from Northern Ecuador. *Amphibian & Reptile Conservation*, 8, 107–120.

Schluter, D. (1988). Character displacement and the adaptive divergence of finches on Island and continents. *The American Naturalist*, 131, 229–249.

Song, J., & Parenti, L. (1995). Clearing and staining whole fish specimens for simultaneous demonstration of bone, cartilage, and nerve. *Copeia*, 1995, 114–118.

Strong, C. R. C., Palci, A., & Caldwell, M. W. (2021). Insights into skull evolution in fossorial snakes, as revealed by the cranial morphology of *Atractaspis irregularis* (Serpentes: Colubroidea). *Journal of Anatomy*, 238, 146–172.

Taylor, W. R., & Van Dyke, G. C. (1985). Revised procedures for staining and clearing small fishes and other vertebrates for bone and cartilage study. *Cybium*, 9, 107–119.

Thomas, R. (1965). The genus *Leptotyphlops* in the West Indies with the description of a new species from Hispaniola (Serpentes, Leptotyphlopidae). *Breviora*, 222, 1–12.

Thomas, R., McDiarmid, R. W., & Thompson, F. G. (1985). Three new species of thread snakes (Serpentes, Leptotyphlopidae) from Hispaniola. *Proceedings of the Biological Society of Washington*, 98, 204–220.

Uetz, P., Freed, P., Hosek, J.. (2020). *The reptile database*, Available from http://www.reptile-database.org.

Underwood, G. (1963). *Reptiles of the eastern Caribbean*. Mona: University of the West Indies.

Underwood, G. (1967). *A contribution to the classification of snakes*. London: Trustees of the British Museum.

Van Valen, L. (1973). A new evolutionary law. *Evolutionary Theory*, 1, 1–33.

Vidal, N., Marin, J., Morini, M., Donnellan, S., Branch, W. R., Thomas, R., … Hedges, S. B. (2010). Blindsnake evolutionary tree reveals long history on Gondwana. *Biology Letters*, 2010, 1–4.

Vonk, F. J., Admiraal, J. F., Jackson, K., Reshef, R., de Bakker, M. A. G., Vanderschoot, K., … Richardson, M. K. (2008). Evolutionary origin and development of snake fangs. *Nature*, 454, 630–633.

Wallach V. (1998a). *The visceral anatomy of Blindsnakes and Wormsnakes and its systematic implications (Serpentes: Anomalepididae, Typhlopidae, Leptotyphlopidae)*. (Unpublished Thesis). Boston.

Wallach, V. (1998b). The lungs of snakes. In C. Gans & A. S. Gaunt (Eds.), *Biology of reptilia* (Vol. 19, pp. 93–295). New York: Society for the Study of Amphibians and Reptiles.

Wallach, V., Williams, K. L., & Boundy, J. (2014). *Snakes of the world: A catalogue of living and extinct species*. Florida: CRC Press.

Wallach, V., & Ineich, I. (1996). Redescription of a rare Malagasy blind snake, Typhlops grandieri Mocquard, with placemet in a new genus (Serpentes: Typhlopidae). *Journal of Herpetology*, 30, 367–376.

Wallach, V., & Gunther, R. (1997). Visceral anatomy of the Malaysian snake genus Xenophidion, with allocation to a new family (SErpentes: Xenophiidae). *Amphibia-Reptilia*, (19), 385–404.

Wallach, V., & Smith, H. (1992). Boella tenella is Epicrates inornatus (Reptilia: Serpentes). *Bulletin Maryland Herpetological Society*, *28*, 162–170.

Winchester, L., & Bellairs, A. (1977). Aspects of vertebral development in lizards and snakes. *Journal of Zoology*, *181*, 495–525.

Yeh, J. (2002). The effect of miniaturized body size on skeletal morphology in frogs. *Evolution*, *2002*, 628–641.

APPENDIX A: MATERIAL EXAMINED

[1] μCT.
[2] X-Ray.
[3] Cleared and stained.
[4] Viscera.

Mitophis asbolepis ($n = 1$). **DOMINICAN REPUBLIC**: BARAHONA: *Loma del Aguacate*: USNM 236660[2](Paratype).

Mitophis calypso ($n = 2$). **DOMINICAN REPUBLIC**: SAMANA: *Las Galeras*: USNM 236658[2](Paratype), 236659[2](Holotype).

Mitophis leptepileptus ($n = 7$). **HAITI**: SUD-EST: *Soliette*: KU 275542[2], 275543[2], 275548[3,4], 275549[2], 275567[2], USNM576217[1]; *Fond Verettes*: USNM 236661[2](Holotype).

Mitophis pyrites ($n = 2$). **DOMINICAN REPUBLIC**: PEDERNALES: *Pedernales*: MCZ 77239[2](Holotype), USNM 152452[2](Paratype).

Tetracheilostoma bilineata ($n = 8$) **MARTINIQUE**: *No Locality*: BMNH 1853.2.4.36[1], MNHN 1994.1147[1](Syntype), ZMB 5056[1]; LE LAMENTIN: *No Locality*: USNM 564808[1,2,4], 564809[2,4]. **SANTA LUCIA**: SANTA LUCIA: *Anse-La-Raye*: USNM 222954[2]; *No locality*: MCZ 10693[4]. **JAMAICA**: *No Locality*: ZMB 4116[1].

Tetracheilostoma breuili ($n = 8$). **SANTA LUCIA**: ILHAS MARIA: *Ilha Maria Major*: USNM 564810[2](Holotype), 564,811–17[2](Paratype).

Tetracheilostoma carlae ($n = 3$). **BARBADOS**: SAINT JOSEPH: *Bonwell*: USNM564818[2](Paratype), 564819[2](Holotype); SAINT JOHN: *Codrington College*: BMNH 1969.792[1](Paratype).